Deep-Space Optical Transceiver Uplink Detection Analysis

Andre Tkacenko*, Kevin J. Quirk*, and Meera Srinivasan*

In this memo, we develop and analyze an uplink signal detection technique for the Deep-Space Optical Transceiver (DOT). Here, the detection is carried out using a set of test statistics obtained from up-down counter (UDC) photon detection systems. Specifically, we address two sets of statistics: the count outputs from a bank of uniformly temporally spaced UDCs as well as the counts from a single UDC that cycles through multiple timing phases. From these test statistics, we derive the Neyman-Pearson decision rule under certain input conditions and analyze the performance of this hypothesis test. We show the performance trade-offs associated with both sets of test statistics, which can then be used to determine which set to use as well as the number of UDCs or timing phases required for implementation.

I. Introduction

In order to receive an uplink communication from an Earth-based beacon, the Deep-Space Optical Transceiver (DOT) flight terminal will use a focal plane array [1] of photon counting detector pixels (possibly of size 128×128). While the Earth and beacon together will occupy a varying amount of pixels depending upon the distance between the DOT and Earth, the system is designed for the beacon to occupy a certain minimum region of pixels (possibly 2×2). This is illustrated in Fig. 1.

For spatial acquisition, the DOT flight terminal will employ up-down counter (UDC) photon detection systems at each pixel. Using UDCs provides a low complexity detection method when combined with appropriate modulation to be able to distinguish between uplink telemetry from the beacon on Earth and background illumination from the Earth as well as ambient background illumination. When a telemetry waveform is incident on a pixel, the UDCs will tend to yield a non-zero output, whereas when only background

*Communication Architectures and Research Section

The research described in this publication was carried out by the Jet Propulsion Laboratory, California Institute of Technology, under a contract with the National Aeronautics and Space Administration.

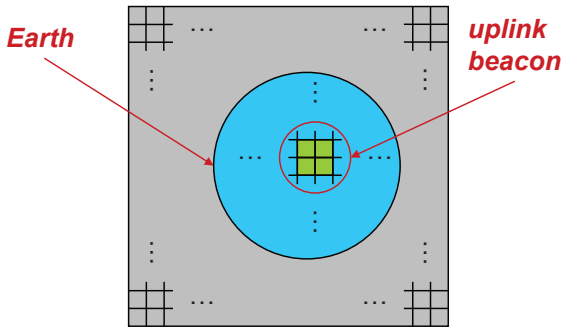

Figure 1. DOT focal plane array with Earth and the uplink beacon present.

illumination is received, the UDCs will have a zero net count on average. As the symbol timing offset of the uplink beacon telemetry waveform will not be known to the DOT *a priori*, UDC count statistics at several timing phases will be required in general. Two ways in which this can be accommodated and which we will analyze here are as follows. Either a bank of uniformly temporally spaced UDCs can be used or a single UDC can be used multiple times at uniformly spaced timing phases. For either case, the temporal spacing is with respect to the uplink symbol interval, which is assumed to be known at the DOT.

A. Outline

In Sec. I-B, we describe the notations that will be used in this memo, whereas in Sec. I-C, we provide a convenient list of terms that will be used throughout the paper. An overview of the uplink detection signal model that we will be focusing on here is provided in Sec. II. In Sec. III, we detail the UDC test statistics that will be considered here and introduce the chip interval counts used to canonically describe them. The probabilistic modeling of the chip interval counts is derived in Sec. III-A, which is then used to determine the probabilistic modeling of the multiple UDC, single phase and single UDC, multiple phase statistics in Secs. III-B and III-C, respectively. A description of the Neyman-Pearson hypothesis test that will be used for detection is given in Sec. IV, along with a symbol timing offset conditional variant as detailed in Sec. IV-A. In Sec. V, we analyze several important special cases of the unconditional Neyman-Pearson hypothesis test, including the single UDC, single phase case in Sec. V-A, the dual UDC, single phase case in Sec. V-B, and the single UDC, dual phase case in Sec. V-C. There, we see the difficulties in deriving the unconditional Neyman-Pearson hypothesis test in general and shift our focus to detection tests conditioned on the symbol timing offset. Specifically, in Sec. VI, we analyze the detection performance for a worst case scenario (WCS) symbol timing offset for both the multiple UDC, single phase system in Sec. VI-A as well as the single UDC, multiple phase system in Sec. VI-B. In Sec. VII, we touch on some of the pros and cons between the two proposed UDC-based uplink signal detection schemes. Concluding remarks are made in Sec. VIII. Finally, in the Appendix, we simplify a certain multivariate Gaussian distribution [2] integral over a hyperspherical region, a result which is used to assess the WCS symbol timing offset detection performance.

B. Notations

Most notations are as in [2]. In particular, parentheses and subscripts are respectively used to denote continuous and discrete function arguments. For example, $g(x)$ would denote a continuous function for $x \in \mathbb{R}$, whereas h_n would denote a discrete function for $n \in \mathbb{Z}$.

Vector/matrix notations are as in [3]. Specifically, boldface lowercase letters (such as $\mathbf{v}$) are used to denote vectors, whereas boldface uppercase letters (such as $\mathbf{A}$) represent matrices. The k-th component of a vector $\mathbf{v}$ will be denoted $[\mathbf{v}]_k$, whereas the (k,ℓ)-th element of a matrix $\mathbf{A}$ is denoted as $[\mathbf{A}]_{k,\ell}$. In addition, the transpose operator will be represented by the superscript ^{T} and the determinant of a square matrix $\mathbf{S}$ is expressed as $\det(\mathbf{S})$.

Random variables are denoted via a non-italicized font, while instances of random variables are expressed using an italicized font. As an example, v may denote a random variable, whereas an instance of v would be expressed as v. Vectors are denoted using a bold font. For example, $\mathbf{v}$ may denote a random vector, while $\boldsymbol{v}$ would denote an instance of $\mathbf{v}$.

A probability density function (pdf) [2] will be denoted by the letter f subscripted by the random variable or vector. For instance, $f_{\mathrm{v}}(v)$ and $f_{\mathbf{v}}(\boldsymbol{v})$ would denote pdfs of the random variable v and random vector $\mathbf{v}$, respectively.

The notation $\mathcal{N}(\mu,\sigma^2)$ will be used to denote a random variable with a normal or Gaussian distribution [2] with mean μ and variance σ^2. If a random variable v has such a distribution, we will write $\mathrm{v} \sim \mathcal{N}(\mu,\sigma^2)$. We will use $\phi(x)$ and $\Phi(x)$ to respectively denote the pdf and cumulative distribution function (cdf) [2] of the *standard normal distribution* [2] (i.e., $\mathcal{N}(0,1)$). These are given by the following expressions [2]:

$$\phi(x) \triangleq \frac{1}{\sqrt{2\pi}} e^{-\frac{x^2}{2}}\,,\;\; \Phi(x) \triangleq \int_{-\infty}^{x} \phi(y)\; dy = \frac{1}{\sqrt{2\pi}} \int_{-\infty}^{x} e^{-\frac{y^2}{2}}\; dy\,.$$

It can be shown that if $\mathrm{x} \sim \mathcal{N}(\mu,\sigma^2)$ and $f_{\mathrm{x}}(x)$ and $F_{\mathrm{x}}(x)$ denote, respectively, the pdf and cdf of x, then we have [2]

$$f_{\mathrm{x}}(x) = \frac{1}{\sigma}\phi\left(\frac{x-\mu}{\sigma}\right)\,,\;\; F_{\mathrm{x}}(x) = \Phi\left(\frac{x-\mu}{\sigma}\right)\,. \tag{1}$$

Similar to the univariate case, the notation $\mathcal{N}_p(\boldsymbol{\mu},\boldsymbol{\Sigma})$ will be used to denote a $p \times 1$ random vector with a multivariate normal or Gaussian distribution [2] with $p \times 1$ mean vector $\boldsymbol{\mu}$ and $p \times p$ covariance matrix $\boldsymbol{\Sigma}$. If a random vector $\mathbf{v}$ has such a distribution, we will write $\mathbf{v} \sim \mathcal{N}_p(\boldsymbol{\mu},\boldsymbol{\Sigma})$. In this case, we have [2]

$$f_{\mathbf{v}}(\boldsymbol{v}) = \frac{1}{(2\pi)^{\frac{p}{2}}\left(\det(\boldsymbol{\Sigma})\right)^{\frac{1}{2}}} e^{-\frac{1}{2}(\boldsymbol{v}-\boldsymbol{\mu})^T\boldsymbol{\Sigma}^{-1}(\boldsymbol{v}-\boldsymbol{\mu})}\,. \tag{2}$$

Finally, we will use the notation $F_{NC\chi^2}(x;p,\lambda)$ to denote the cdf of a noncentral chi-square distribution with p degrees of freedom and non-centrality parameter λ evaluated at x [4]. In addition, we will use the notation $F^{-1}_{NC\chi^2}(P;p,\lambda)$ to denote the *quantile* function [2] (i.e., the inverse of the cdf) of a noncentral chi-square distribution with p degrees of freedom and non-centrality parameter λ evaluated at P.

C. Summary of Terms

A list of frequently used terms is provided below for convenience.

M	–	pulse position modulation (PPM) [1, 5] data symbol order,
P	–	number of inter-symbol guard time (ISGT) [6] slots used,
G	–	number of UDCs in a multiple UDC, single phase system or the number of timing phases of a single UDC, multiple phase system,
λ_s	–	average detected signal photon arrival rate,
λ_b	–	average detected background and dark [1] photon arrival rate,
T_s	–	slot time interval,
K_s	–	mean number of signal photon counts per signal slot (i.e., $K_s \triangleq \lambda_s (M+P) T_s$),
K_b	–	mean number of background photon counts per slot (i.e., $K_b \triangleq \lambda_b T_s$),
N_{sym}	–	number of symbols observed for a multiple UDC, single phase system,
N_{spp}	–	number of symbols per timing phase observed for a single UDC, multiple phase system,
T_{sym}	–	symbol time interval (i.e., $T_{\mathrm{sym}} \triangleq (M+P) T_s$),
T_d	–	detection time interval (i.e., $T_d = N_{\mathrm{sym}} T_{\mathrm{sym}}$ for a multiple UDC, single phase system and $T_d = N_{\mathrm{spp}} G T_{\mathrm{sym}}$ for a single UDC, multiple phase system).

II. Uplink Detection Signal Model

The uplink signal model is characterized by a received photon intensity function, which we denote here by $i(t)$. From UDC test statistics based upon this received signal, we must infer whether or not telemetry has been sent. For the DOT, we assume that a transmitted telemetry signal will consist of symbols, each formed from the concatenation of the following components:

- an M-ary PPM data symbol,
- a set of P ISGTs.

Whether or not a telemetry signal was transmitted, we will assume that there is a background illumination present at the receiver. This leads to the following expression for the received laser intensity waveform $i(t)$:

$$i(t) = \begin{cases} \lambda_s (M+P) \left[\sum_{n=-\infty}^{\infty} p\Big(\frac{t}{T_s} - \epsilon - d_n - (M+P)\, n \Big) \right] + \lambda_b \,, & \text{telemetry present} \\ \lambda_b \,, & \text{telemetry absent} \end{cases} , \tag{3}$$

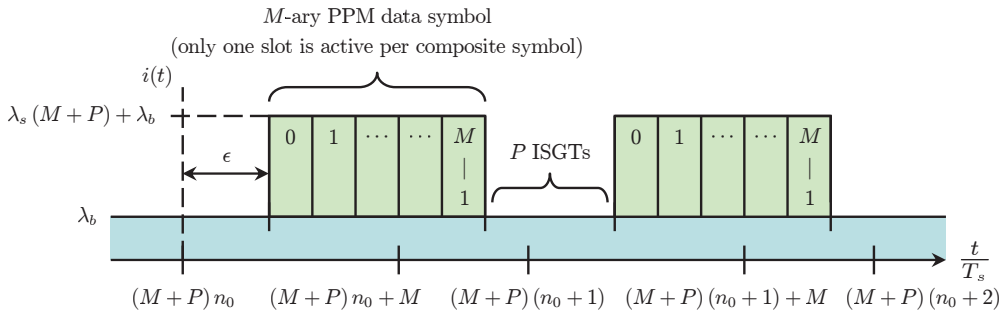

Figure 2. Sample plot of the received photon intensity waveform $i(t)$ when telemetry is present.

where we have

$\epsilon \triangleq$ symbol timing offset (normalized by T_s),
In general, we have $\epsilon_0 \leq \epsilon < \epsilon_0 + (M+P)$ for any $\epsilon_0 \in \mathbb{R}$.

$\{d_n\} \triangleq$ M-ary PPM data sequence,
Here, $d_n \in \{0, 1, \ldots, M-1\}$.
Also, we will assume that $\{d_n\}$ is an independent, identically distributed (iid or i.i.d.) sequence [2] with
$\Pr\{d_n = m\} = \dfrac{1}{M}\,,\ \forall\ 0 \leq m \leq M-1,\ n \in \mathbb{Z}\,.$

$p(x) \triangleq$ telemetry transmit pulse shape.
Here, we assume $p(x)$ is rectangular as follows:

$$p(x) = \begin{cases} 1\,, & 0 \leq x < 1 \\ 0\,, & \text{otherwise} \end{cases}\,.$$

A sample plot of the received photon intensity signal $i(t)$ in the case of telemetry being present is shown in Fig. 2. As only one of the M-ary PPM data slots will be active for each composite symbol, consisting of $(M+P)$ slot intervals total, it follows that the average signal arrival rate will be λ_s.

Another signal of interest which will simplify subsequent statistical analysis of the UDC hypothesis test metrics will be the photon intensity function averaged over the random PPM data. This signal, which we will denote by $\bar{i}(t)$, is given by the following expression:

$$\bar{i}(t) = \begin{cases} \lambda_s \dfrac{(M+P)}{M} \displaystyle\sum_{n=-\infty}^{\infty} p\left(\frac{\frac{t}{T_s} - \epsilon - (M+P)\,n}{M}\right) + \lambda_b\,, & \text{telemetry present} \\ \lambda_b\,, & \text{telemetry absent} \end{cases}\,. \quad (4)$$

A sample plot of the data-averaged received photon intensity function $\bar{i}(t)$ when telemetry is present is shown in Fig. 3. As can be seen, $\bar{i}(t)$ is similar to $i(t)$ as shown in Fig. 2, except that the random data present in $i(t)$ is averaged to produce the wide non-random rectangular pulse present in $\bar{i}(t)$. The signal component of this wide pulse has an amplitude which is M times smaller than that when random data is present, due to averaging of the data.

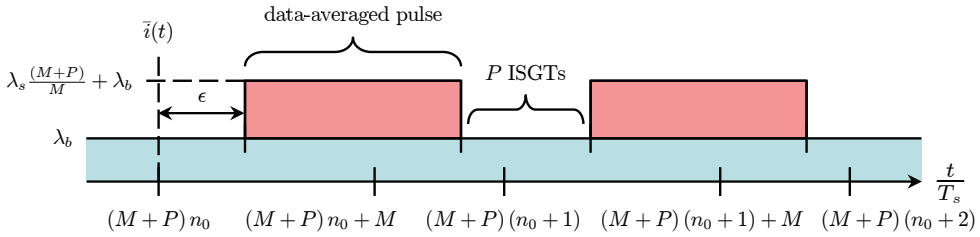

Figure 3. Sample plot of the data-averaged received photon intensity waveform $\bar{i}(t)$ with telemetry present.

III. Up-Down Counter Test Statistics

As mentioned above, the uplink detection problem is to determine whether or not a telemetry signal was transmitted. Thus, from (3) we have two hypotheses as described below:

$$\begin{aligned} H_0 \quad &: \quad i(t) = \lambda_b \\ H_1 \quad &: \quad i(t) = \lambda_s\,(M+P)\left[\sum_{n=-\infty}^{\infty} p\!\left(\frac{t}{T_s} - \epsilon - d_n - (M+P)\,n\right)\right] + \lambda_b \end{aligned} \quad , \tag{5}$$

where, H_0 and H_1 correspond, respectively, to the cases in which telemetry is absent and present. We will refer to H_0 as the *null hypothesis*, whereas H_1 will be referred to as the *present hypothesis*.

Here, a decision will be made as to whether H_0 or H_1 is true based on one of two possible sets of G UDC statistics. For the multiple UDC, single phase case, the test statistics will consist of the count outputs of a bank of G uniformly temporally staggered UDCs, whereas for the single UDC, multiple phase case, the test statistics will consist of the count outputs of a single UDC applied G times at uniformly spaced timing offset phases.

To formally introduce both sets of test statistics, let us first define the following chip time interval T_c:

$$T_c \triangleq \frac{T_{\rm sym}}{2G} = \frac{(M+P)\,T_s}{2G} \quad \text{(chip time interval)}\,. \tag{6}$$

Then, let us define the random variable N_k as follows:

$$\mathrm{N}_k \triangleq \#\text{ of photon counts over the time interval } t \in [kT_c, (k+1)T_c)\,,\ \forall\ k \in \mathbb{Z}\,. \tag{7}$$

From these count random variables, we form our G UDC test statistics for both the multiple UDC, single phase and single UDC, multiple phase cases. Let $N_{\rm sym}$ and $N_{\rm spp}$ denote, respectively, the number of symbols observed for the multiple UDC, single phase case and the number of symbols per phase observed for the single UDC, multiple phase case (see Sec. I-C). The UDC test statistics $\{\mathrm{g}_\ell\}_{\ell=0}^{G-1}$ for both cases are then

$$\mathrm{g}_\ell \triangleq \begin{cases} \dfrac{1}{N_{\rm sym}} \displaystyle\sum_{q=0}^{N_{\rm sym}-1} \sum_{r=0}^{(2G)-1} (-1)^{\left\lfloor \frac{r-\ell}{G} \right\rfloor} \mathrm{N}_{(2G)q+r}\,, & \text{(multiple UDC, single phase case)} \\ \dfrac{1}{N_{\rm spp}} \displaystyle\sum_{q=0}^{N_{\rm spp}-1} \sum_{r=0}^{(2G)-1} (-1)^{\left\lfloor \frac{r-\ell}{G} \right\rfloor} \mathrm{N}_{(2G)(q+\ell N_{\rm spp})+r}\,, & \text{(single UDC, multiple phase case)} \end{cases} \tag{8}$$

.

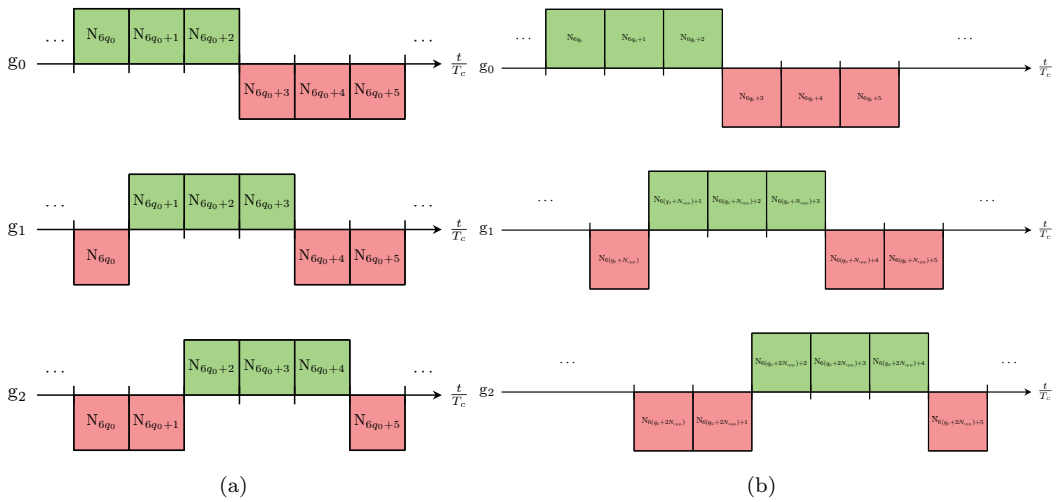

Figure 4. Pictorial view of the formation of the UDC test statistics for $G = 3$: (a) multiple UDC, single phase case and (b) single UDC, multiple phase case (up counts in green and down counts in red).

A pictorial view of how the UDC statistics are formed in both cases is shown for $G = 3$ in Fig. 4. As can be seen from Fig. 4(a), for the multiple UDC, single phase case, the statistics overlap in time, whereas from Fig. 4(b), for the single UDC, multiple phase case, there is no temporal overlap of the test statistics. For both cases, however, it is evident that the test statistics represent G time intervals uniformly offset across the total symbol interval length T_{sym}.

A comment is in order here regarding the single UDC, multiple phase test statistics from (8). By construction, these statistics span contiguous, non-overlapping time intervals. Specifically, from (8), (7), and (6), it can be seen that g_ℓ represents up-down photon counts over the time interval $t \in [\ell N_{\text{spp}} T_{\text{sym}}, (\ell + 1) N_{\text{spp}} T_{\text{sym}})$, the set of which, for all ℓ, is contiguous and non-overlapping. However, as will be seen subsequently in Sec. III-C, the probabilistic characterization of this set of test statistics will be the same as those for which the time intervals are only non-overlapping. Hence, instead of the contiguous and non-overlapping single UDC, multiple phase statistics from (8), we could also use a set of test statistics that are only non-overlapping. In essence, there is no loss of generality in assuming a contiguous form as in (8) and this was merely chosen as such here for notational simplicity.

For notational convenience, we will define the $G \times 1$ random vector $\mathbf{g}$ to be the vector of UDC test statistics given by

$$\mathbf{g} \triangleq \begin{bmatrix} \mathrm{g}_0 & \mathrm{g}_1 & \cdots & \mathrm{g}_{G-1} \end{bmatrix}^T. \tag{9}$$

In accordance with the notational conventions adopted here (see Sec. I-B), we will denote an instance of $\mathbf{g}$ by $\boldsymbol{g}$.

A. Probabilistic Modeling of the Chip Interval Counts

The photon detection counting process [1] is assumed to be a *Poisson process* [2]. Let λ_k denote the average arrival rate [1] corresponding to the chip count variable N_k. From (7), we have

$$\lambda_k \triangleq \frac{1}{T_c} \int_{kT_c}^{(k+1)T_c} i(t)\ dt\,, \tag{10}$$

where $i(t)$ is as in (3). Conditioned on λ_k, it follows that N_k is *Poisson* with mean $\lambda_k T_c$. Specifically, this means that we have [2]

$$\Pr\{\mathrm{N}_k = m \,|\, \lambda_k\} = \frac{(\lambda_k T_c)^m\, e^{-(\lambda_k T_c)}}{m!} u_m\,,\ m \in \mathbb{Z}\,,$$

where u_m is the *Heaviside step sequence* [2]. Furthermore, as N_k and N_ℓ represent counts across non-overlapping time intervals for all $k \neq \ell$ (as evidenced from (7)), it follows that $\mathrm{N}_k \,|\, \lambda_k$ and $\mathrm{N}_\ell \,|\, \lambda_\ell$ are independent for all $k \neq \ell$.

When telemetry is present, it can be shown that the arrival rate λ_k will be a deterministic function of the symbol timing offset ϵ, when averaged over the random PPM data. For the case in which telemetry is absent, it follows that $\lambda_k = \lambda_b$ and so it is trivially a deterministic function of ϵ. Thus, analogously to (10), if we define the average arrival rate $\overline{\lambda}_k(\epsilon)$ for both the null and present hypotheses as

$$\overline{\lambda}_k(\epsilon) \triangleq \frac{1}{T_c} \int_{kT_c}^{(k+1)T_c} \overline{i}(t)\ dt\,, \tag{11}$$

where $\overline{i}(t)$ is as in (4), then we have

$$\mathrm{N}_k \,|\, \epsilon \sim \mathrm{Poisson}\big(\overline{\lambda}_k(\epsilon)\, T_c\big)\ . \tag{12}$$

In other words, the random variable $\mathrm{N}_k \,|\, \epsilon$ is Poisson with mean $\overline{\lambda}_k(\epsilon)\, T_c$. Furthermore, as N_k and N_ℓ represent non-overlapping count time intervals for all $k \neq \ell$, it follows that $\mathrm{N}_k \,|\, \epsilon$ and $\mathrm{N}_\ell \,|\, \epsilon$ are independent for all $k \neq \ell$.

One noteworthy property of $\overline{\lambda}_k(\epsilon)$ that can be deduced from (11) and (4) is that

$$\overline{\lambda}_k(\epsilon) = \overline{\lambda}_{k \bmod (2G)}(\epsilon)\ ,\ \forall\ k \in \mathbb{Z}\,. \tag{13}$$

This follows from the fact that $\overline{i}(t)$ is periodic with period $T_{\mathrm{sym}} = (2G)\, T_c$ (for both hypotheses) and that the integration region in (11) is over an interval of length T_c. This implies that there are at most $(2G)$ distinct values of $\overline{\lambda}_k(\epsilon)$ for fixed ϵ. As such, from (12) and (13), we have the following:

$$\mathrm{N}_k \,|\, \epsilon \sim \mathrm{Poisson}\big(\overline{\lambda}_{k \bmod (2G)}(\epsilon)\, T_c\big)\ . \tag{14}$$

In other words, as k varies, the distribution of the count variable N_k, conditioned on the symbol timing offset ϵ, is only a function of the *remainder* of k when divided by $(2G)$.

B. Probabilistic Modeling of the Multiple UDC, Single Phase Statistics

To statistically characterize the multiple UDC, single phase test statistics from (8), note that we can express the normalized count random variable g_ℓ as

$$\mathrm{g}_\ell = \sum_{r=0}^{(2G)-1} (-1)^{\left\lfloor \frac{r-\ell}{G} \right\rfloor} \mathrm{C}_r \,, \text{ where } \mathrm{C}_r \triangleq \frac{1}{N_{\mathrm{sym}}} \sum_{q=0}^{N_{\mathrm{sym}}-1} \mathrm{N}_{(2G)q+r} \,. \tag{15}$$

Now, to analyze the random variable C_r, first note that from (14) that

$$\mathrm{N}_{(2G)q+r} \,|\, \epsilon \sim \text{Poisson}\big(\overline{\lambda}_r(\epsilon)\, T_c\big) \,.$$

In other words, for fixed r, $\big\{\mathrm{N}_{(2G)q+r} \,|\, \epsilon\big\}_{q=0}^{N_{\mathrm{sym}}-1}$ have identical distribution. Furthermore as $\big\{\mathrm{N}_{(2G)q+r} \,|\, \epsilon\big\}_{q=0}^{N_{\mathrm{sym}}-1}$ are independent, it follows $\big\{\mathrm{N}_{(2G)q+r} \,|\, \epsilon\big\}_{q=0}^{N_{\mathrm{sym}}-1}$ are iid. As the variance of $\mathrm{N}_{(2G)q+r} \,|\, \epsilon$ is equal to $\overline{\lambda}_r(\epsilon)\, T_c$ (since $\mathrm{N}_{(2G)q+r} \,|\, \epsilon$ is Poisson with mean $\overline{\lambda}_r(\epsilon)\, T_c$ [2]), it follows by the *central limit theorem* [2] that for large N_{sym}, we have

$$\mathrm{C}_r \,|\, \epsilon \sim \mathcal{N}\left(\overline{\lambda}_r(\epsilon)\, T_c, \frac{\overline{\lambda}_r(\epsilon)\, T_c}{N_{\mathrm{sym}}}\right) \,. \tag{16}$$

Furthermore, as C_r is formed from non-overlapping count random variables for varying r as evident from (15), it follows that $\mathrm{C}_k \,|\, \epsilon$ and $\mathrm{C}_\ell \,|\, \epsilon$ are independent for all $k \neq \ell$, where $k, \ell \in \{0, 1, \ldots, (2G)-1\}$.

To further simplify the probabilistic model of the multiple UDC, single phase test statistics, note that from (15) that we have the following:

$$\begin{aligned}
\mathrm{g}_\ell &= \sum_{r=0}^{G-1} (-1)^{\left\lfloor \frac{r-\ell}{G} \right\rfloor} \mathrm{C}_r + \sum_{r=G}^{(2G)-1} (-1)^{\left\lfloor \frac{r-\ell}{G} \right\rfloor} \mathrm{C}_r \,, \\
&= \sum_{r=0}^{G-1} (-1)^{\left\lfloor \frac{r-\ell}{G} \right\rfloor} \mathrm{C}_r + \sum_{m=0}^{G-1} (-1)^{\left\lfloor \frac{m-\ell}{G}+1 \right\rfloor} \mathrm{C}_{G+m} \,, &(17)\\
&= \sum_{r=0}^{G-1} (-1)^{\left\lfloor \frac{r-\ell}{G} \right\rfloor} \mathrm{C}_r - \sum_{r=0}^{G-1} (-1)^{\left\lfloor \frac{r-\ell}{G} \right\rfloor} \mathrm{C}_{G+r} = \sum_{r=0}^{G-1} (-1)^{\left\lfloor \frac{r-\ell}{G} \right\rfloor} (\mathrm{C}_r - \mathrm{C}_{G+r}) \,, &(18)\\
&= \sum_{r=0}^{G-1} (-1)^{\left\lfloor \frac{r-\ell}{G} \right\rfloor} \mathrm{D}_r \,, \text{ where } \mathrm{D}_r \triangleq \mathrm{C}_r - \mathrm{C}_{G+r} \,,\ 0 \leq r \leq G-1 \,. &(19)
\end{aligned}$$

Here, (17) follows from the substitution $m = r - G$ in the second summation and (18) follows from the fact that $\lfloor x + n \rfloor = \lfloor x \rfloor + n$ for any $n \in \mathbb{Z}$ [7]. From (16) and the fact that $\mathrm{C}_r \,|\, \epsilon$ and $\mathrm{C}_{G+r} \,|\, \epsilon$ are independent for all $0 \leq r \leq G-1$, it can be shown that we have [2]

$$\mathrm{D}_r \,|\, \epsilon \sim \mathcal{N}\left(\big(\overline{\lambda}_r(\epsilon) - \overline{\lambda}_{G+r}(\epsilon)\big)\, T_c, \frac{\big(\overline{\lambda}_r(\epsilon) + \overline{\lambda}_{G+r}(\epsilon)\big)\, T_c}{N_{\mathrm{sym}}}\right) \,. \tag{20}$$

Furthermore, from (19), it can be seen that $\mathrm{D}_k \,|\, \epsilon$ and $\mathrm{D}_\ell \,|\, \epsilon$ are independent for all $k \neq \ell$ with $k, \ell \in \{0, 1, \ldots, G-1\}$.

Returning to the multiple UDC, single phase test statistics, note that from (19) that we have the following:

$$\mathrm{D}_\ell = \begin{cases} \dfrac{\mathrm{g}_\ell - \mathrm{g}_{\ell+1}}{2}\,, & 0 \le \ell \le G-2 \\ \dfrac{\mathrm{g}_{G-1} + \mathrm{g}_0}{2}\,, & \ell = G-1 \end{cases} . \tag{21}$$

Conditioned on the symbol timing offset ϵ, the relationship given in (21) expresses the multiple UDC, single phase test statistics $\{\mathrm{g}_\ell\}_{\ell=0}^{G-1}$ in terms of a set of independent Gaussian random variables, namely $\{\mathrm{D}_\ell \,|\, \epsilon\}_{\ell=0}^{G-1}$. Also, as the mapping between $\{\mathrm{g}_\ell\}_{\ell=0}^{G-1}$ and $\{\mathrm{D}_\ell\}_{\ell=0}^{G-1}$ is one-to-one [2], they are equivalent sets of statistics [8]. Hence, $\{\mathrm{D}_\ell\}_{\ell=0}^{G-1}$ represents a canonical decomposition of the multiple UDC, single phase test statistics and will be used for all subsequent analysis here for this case.

To formally introduce the canonical multiple UDC, single phase test statistics, we will define the $G \times 1$ random vector $\mathbf{D}$ as

$$\mathbf{D} \triangleq \begin{bmatrix} \mathrm{D}_0 & \mathrm{D}_1 & \cdots & \mathrm{D}_{G-1} \end{bmatrix}^T . \tag{22}$$

From (21) and (9), we can express $\mathbf{D}$ in (22) as follows:

$$\mathbf{D} = \mathbf{A}\mathbf{g}\,,$$

where $\mathbf{A}$ is the $G \times G$ matrix

$$\mathbf{A} \triangleq \begin{bmatrix} \frac{1}{2} & -\frac{1}{2} & 0 & \cdots & 0 \\ 0 & \frac{1}{2} & -\frac{1}{2} & \ddots & \vdots \\ \vdots & \ddots & \ddots & \ddots & 0 \\ 0 & \cdots & 0 & \frac{1}{2} & -\frac{1}{2} \\ \frac{1}{2} & 0 & \cdots & 0 & \frac{1}{2} \end{bmatrix} .$$

In summary, from (20), the canonical multiple UDC, single phase test statistic vector $\mathbf{D}$ from (22) satisfies

$$\mathbf{D} \,|\, \epsilon \sim \mathcal{N}_G\Big(\boldsymbol{\mu}_{\mathbf{D}|\epsilon}, \boldsymbol{\Sigma}_{\mathbf{D}|\epsilon}\Big)\,, \tag{23}$$

where we have

$$\Big[\boldsymbol{\mu}_{\mathbf{D}|\epsilon}\Big]_k = \big(\overline{\lambda}_k(\epsilon) - \overline{\lambda}_{G+k}(\epsilon)\big)\, T_c\,,\ 0 \le k \le G-1\,, \tag{24}$$

$$\big[\boldsymbol{\Sigma}_{\mathbf{D}|\epsilon}\big]_{k,\ell} = \begin{cases} \dfrac{\big(\overline{\lambda}_k(\epsilon) + \overline{\lambda}_{G+k}(\epsilon)\big)\, T_c}{N_{\mathrm{sym}}}\,, & k = \ell \\ 0\,, & k \ne \ell \end{cases} ,\ 0 \le k, \ell \le G-1\,. \tag{25}$$

Conforming to the notational conventions used here, we will denote an instance of $\mathbf{D}$ by $\boldsymbol{D}$.

C. Probabilistic Modeling of the Single UDC, Multiple Phase Statistics

Analogous to the multiple UDC, single phase case, to statistically characterize the single UDC, multiple phase test statistics from (8), note that we can express the normalized

count random variable g_ℓ as

$$\mathrm{g}_\ell = \sum_{r=0}^{(2G)-1} (-1)^{\left\lfloor \frac{r-\ell}{G} \right\rfloor} \mathrm{C}_{\ell,r}\,, \text{ where } \mathrm{C}_{\ell,r} \triangleq \frac{1}{N_{\mathrm{spp}}} \sum_{q=0}^{N_{\mathrm{spp}}-1} \mathrm{N}_{(2G)(q+\ell N_{\mathrm{spp}})+r}\,. \tag{26}$$

As with the random variable C_r defined in (15), the central limit theorem can be applied to $\mathrm{C}_{\ell,r}$ conditioned on the symbol timing offset ϵ, for large N_{spp}. In this case, we have

$$\mathrm{C}_{\ell,r} \,|\, \epsilon \sim \mathcal{N}\left(\overline{\lambda}_r(\epsilon)\, T_c, \frac{\overline{\lambda}_r(\epsilon)\, T_c}{N_{\mathrm{spp}}} \right)\,. \tag{27}$$

Furthermore, as $\mathrm{C}_{\ell,r}$ is formed from non-overlapping count random variables for varying ℓ and r as evident from (26), it follows that $\mathrm{C}_{\ell_0,r_0} \,|\, \epsilon$ and $\mathrm{C}_{\ell_1,r_1} \,|\, \epsilon$ are independent for all $\ell_0 \neq \ell_1$ or $r_0 \neq r_1$, where $\ell_0, \ell_1 \in \{0, 1, \ldots, G-1\}$ and $r_0, r_1 \in \{0, 1, \ldots, (2G)-1\}$.

To further simplify the probabilistic model of the single UDC, multiple phase test statistics, note that from (26) that we have

$$\mathrm{g}_\ell = \sum_{r=0}^{G-1} (-1)^{\left\lfloor \frac{r-\ell}{G} \right\rfloor} \mathrm{D}_{\ell,r}\,, \text{ where } \mathrm{D}_{\ell,r} \triangleq \mathrm{C}_{\ell,r} - \mathrm{C}_{\ell,G+r}\,,\ 0 \leq \ell, r \leq G-1\,. \tag{28}$$

From (27) and the fact that $\mathrm{C}_{\ell,r} \,|\, \epsilon$ and $\mathrm{C}_{\ell,G+r} \,|\, \epsilon$ are independent for all ℓ and $0 \leq r \leq G-1$, it can be shown that we have [2]

$$\mathrm{D}_{\ell,r} \,|\, \epsilon \sim \mathcal{N}\left(\left(\overline{\lambda}_r(\epsilon) - \overline{\lambda}_{G+r}(\epsilon)\right) T_c, \frac{\left(\overline{\lambda}_r(\epsilon) + \overline{\lambda}_{G+r}(\epsilon)\right) T_c}{N_{\mathrm{spp}}} \right)\,. \tag{29}$$

Furthermore, from (28), it can be seen that $\mathrm{D}_{\ell_0,r_0} \,|\, \epsilon$ and $\mathrm{D}_{\ell_1,r_1} \,|\, \epsilon$ are independent for all $\ell_0 \neq \ell_1$ or $r_0 \neq r_1$, where $\ell_0, \ell_1, r_0, r_1 \in \{0, 1, \ldots, G-1\}$. Using this result in (28), it follows that $\mathrm{g}_k \,|\, \epsilon$ and $\mathrm{g}_\ell \,|\, \epsilon$ are independent for all $k \neq \ell$ with $k, \ell \in \{0, 1, \ldots, G-1\}$. Combining this latest fact with (29), it follows that the single UDC, multiple phase test statistic vector $\mathbf{g}$ from (9) satisfies the following [2]:

$$\mathbf{g} \,|\, \epsilon \sim \mathcal{N}_G\left(\boldsymbol{\mu}_{\mathbf{g}|\epsilon}, \boldsymbol{\Sigma}_{\mathbf{g}|\epsilon} \right)\,, \tag{30}$$

where we have

$$\left[\boldsymbol{\mu}_{\mathbf{g}|\epsilon}\right]_k = \sum_{r=0}^{G-1} (-1)^{\left\lfloor \frac{r-k}{G} \right\rfloor} \left(\overline{\lambda}_r(\epsilon) - \overline{\lambda}_{G+r}(\epsilon)\right) T_c\,,\ 0 \leq k \leq G-1\,, \tag{31}$$

$$\boldsymbol{\Sigma}_{\mathbf{g}|\epsilon} = \left(\sum_{r=0}^{G-1} \frac{\left(\overline{\lambda}_r(\epsilon) + \overline{\lambda}_{G+r}(\epsilon)\right) T_c}{N_{\mathrm{spp}}} \right) \mathbf{I}_G\,. \tag{32}$$

Here, $\mathbf{I}_G$ denotes the $G \times G$ identity matrix [3].

IV. Neyman-Pearson Hypothesis Test

In this setting, a decision will be made as to whether the null or present hypothesis, namely H_0 or H_1 respectively from (5), is true based on the *Neyman-Pearson hypothesis*

test [2, 8]. This test compares the likelihood ratio (or equivalently the log likelihood ratio as we will use here [2]) to a threshold value, which we will denote by η. If the ratio is lower than η, then H_0 is selected, whereas if the ratio exceeds η, then H_1 is chosen. In the event that the ratio equals η, then either H_0 or H_1 is randomly selected according to the prior distribution of the hypotheses, which will either be assumed to be known or modeled as uniformly distributed if not. Specifically for the Neyman-Pearson test, the threshold η is chosen such that the *false alarm probability* [2], which we denote here by P_{FA}, equals some prescribed value, say α. By the *Neyman-Pearson lemma* [2, 8], the such a threshold test is the *most powerful test* [2] of *size* α for a threshold η.

To quantitatively introduce the Neyman-Pearson hypothesis test, we will first formally define the log likelihood ratio. The *log likelihood ratio* $\Lambda(\boldsymbol{x})$ is defined as follows [2]:

$$\Lambda(\boldsymbol{x}) \triangleq \log\left[\frac{f_{\mathbf{x}\,|\,H_1}(\boldsymbol{x})}{f_{\mathbf{x}\,|\,H_0}(\boldsymbol{x})}\right] . \tag{33}$$

In (33), $f_{\mathbf{x}\,|\,H_0}(\boldsymbol{x})$ and $f_{\mathbf{x}\,|\,H_1}(\boldsymbol{x})$ denote, respectively, the pdfs of the observed UDC test statistic vector $\mathbf{x}$ (either $\mathbf{D}$ from (22) for the multiple UDC, single phase case or $\mathbf{g}$ from (9) for the single UDC, multiple phase case) under hypotheses H_0 and H_1. Here, $f_{\mathbf{x}\,|\,H_1}(\boldsymbol{x})$ will be marginalized over the random symbol timing offset, which we will denote here by $\boldsymbol{\varepsilon}$. Specifically, $f_{\mathbf{x}\,|\,H_1}(\boldsymbol{x})$ is calculated as

$$f_{\mathbf{x}\,|\,H_1}(\boldsymbol{x}) = \int_{\mathcal{R}_\varepsilon} f_{\mathbf{x}\,|\,H_1,\boldsymbol{\varepsilon}}(\boldsymbol{x}\,|\,\epsilon)\, f_{\boldsymbol{\varepsilon}}(\epsilon)\; d\epsilon\,, \tag{34}$$

where, $f_{\boldsymbol{\varepsilon}}(\epsilon)$ denotes the pdf of the random symbol timing offset $\boldsymbol{\varepsilon}$ and $\mathcal{R}_{\boldsymbol{\varepsilon}}$ represents the region of support of this pdf. In addition, $f_{\mathbf{x}\,|\,H_1,\boldsymbol{\varepsilon}}(\boldsymbol{x}\,|\,\epsilon)$ denotes the conditional pdf of the UDC test statistic vector $\mathbf{x}$ given the timing offset $\boldsymbol{\varepsilon}$. From the discussion in Sec. II, we will assume here that $\boldsymbol{\varepsilon}$ is uniformly distributed [2] across a symbol interval. With this assumption, without loss of generality, the expression in (34) becomes

$$f_{\mathbf{x}\,|\,H_1}(\boldsymbol{x}) = \frac{1}{(M+P)} \int_0^{(M+P)} f_{\mathbf{x}\,|\,H_1,\boldsymbol{\varepsilon}}(\boldsymbol{x}\,|\,\epsilon)\; d\epsilon\,. \tag{35}$$

With the log likelihood ratio introduced as such, we are now ready to state the Neyman-Pearson hypothesis test. This test is described below as follows [2, 8]:

$$\Lambda(\boldsymbol{x}) \underset{H_0}{\overset{H_1}{\gtrless}} \eta\,, \text{ where } P_{FA} \triangleq \Pr\left\{\Lambda(\boldsymbol{x}) > \eta\,|\,H_0\right\} = \alpha\,. \tag{36}$$

The probability of false alarm can be calculated via the following expression:

$$P_{FA} = \int_{\mathcal{R}_{H_1}} f_{\mathbf{x}\,|\,H_0}(\boldsymbol{x})\; d\boldsymbol{x}\,, \tag{37}$$

where $\mathcal{R}_{H_1}$ is the decision region corresponding to the present hypothesis H_1 defined as

$$\mathcal{R}_{H_1} \triangleq \{\boldsymbol{x} : \Lambda(\boldsymbol{x}) > \eta\}\ . \tag{38}$$

Using (35), (37), and (38), we can derive the Neyman-Pearson hypothesis test in (36) for uplink signal detection. To evaluate the performance of this test, we can compute the

missed detection probability [2, 8], denoted by P_{MD} and given by the following expression:

$$P_{MD} = \int_{\mathcal{R}_{H_0}} f_{\mathbf{x}\,|\,H_1}(\boldsymbol{x})\; d\boldsymbol{x}\,, \tag{39}$$

where $\mathcal{R}_{H_0}$ is the decision region corresponding to the null hypothesis H_0 defined as

$$\mathcal{R}_{H_0} \triangleq \{\boldsymbol{x} : \Lambda(\boldsymbol{x}) < \eta\}\;. \tag{40}$$

The ultimate measure of performance of a hypothesis test would be the *probability of error* [2, 8], denoted by P_E. This can be expressed in terms of the false alarm probability P_{FA} and the probability of missed detection P_{MD} as follows [2]:

$$P_E = P_{FA}P_{H_0} + P_{MD}P_{H_1}\,,$$

where P_{H_0} and P_{H_1} denote, respectively, the *a priori* probabilities of the hypotheses H_0 and H_1. However, as P_{H_0} and P_{H_1} will not be known in general and since the error probability P_E will typically be dominated by the false alarm probability P_{FA} by design here, it will be more insightful to assess the performance of the Neyman-Pearson hypothesis test in terms of the missed detection probability P_{MD} from (39).

A. Symbol Timing Offset Conditional Test

As will be subsequently shown in Sec. V, calculating the log likelihood ratio $\Lambda(\boldsymbol{x})$ from (33) can often be difficult and intractable due to the form of the marginalized pdf $f_{\mathbf{x}\,|\,H_1}(\boldsymbol{x})$ from (34). In such cases, it will be more insightful to derive the Neyman-Pearson hypothesis test conditioned on a specific value of the symbol timing offset, say ϵ_0. For this type of test, we calculate the *conditional* log likelihood $\Lambda(\boldsymbol{x}\,|\,\epsilon_0)$ defined as

$$\Lambda(\boldsymbol{x}\,|\,\epsilon_0) \triangleq \log\left[\frac{f_{\mathbf{x}\,|\,H_1,\varepsilon}(\boldsymbol{x}\,|\,\epsilon_0)}{f_{\mathbf{x}\,|\,H_0}(\boldsymbol{x})}\right]\,. \tag{41}$$

From this, the conditional Neyman-Pearson hypothesis test is given as follows:

$$\Lambda(\boldsymbol{x}\,|\,\epsilon_0) \underset{H_0}{\overset{H_1}{\gtrless}} \eta\,,\;\text{where } P_{FA} \triangleq \Pr\left\{\Lambda(\boldsymbol{x}\,|\,\epsilon_0) > \eta\,|\,H_0\right\} = \alpha\,. \tag{42}$$

The false alarm probability P_{FA} and missed detection probability P_{MD} are then given by

$$P_{FA} = \int_{\mathcal{R}_{H_1}} f_{\mathbf{x}\,|\,H_0}(\boldsymbol{x})\; d\boldsymbol{x}\,,\;\text{where } \mathcal{R}_{H_1} \triangleq \{\boldsymbol{x} : \Lambda(\boldsymbol{x}\,|\,\epsilon_0) > \eta\}\;, \tag{43}$$

and

$$P_{MD} = \int_{\mathcal{R}_{H_0}} f_{\mathbf{x}\,|\,H_1,\varepsilon}(\boldsymbol{x}\,|\,\epsilon_0)\; d\boldsymbol{x}\,,\;\text{where } \mathcal{R}_{H_0} \triangleq \{\boldsymbol{x} : \Lambda(\boldsymbol{x}\,|\,\epsilon_0) < \eta\}\;. \tag{44}$$

In Sec. VI, we derive and assess the performance of the Neyman-Pearson hypothesis test for a worst case symbol timing offset in which the offset lies in between two UDC timing phases.

Table 1. Possible operating point conditions for a Mars-to-Earth communication link.

T_s	65.536 μs
λ_b	1×10^6 p/s
λ_s	50×10^3 p/s

V. Unconditional Hypothesis Test Detection Analysis for Important Special Cases

In this section, we will focus on uplink signal detection using the unconditional Neyman-Pearson hypothesis test for certain special cases for which much of the analysis is tractable. For the DOT uplink signaling format, suggested values for the PPM order and number of ISGT slots have been $M = 2$ and $P = 2$, respectively. These values will be used for the remainder of this article.

A set of possible operating point conditions for a Mars-to-Earth communication link is shown in Tbl. 1. Note that from these values, as well as the suggested PPM order and number of ISGT slots that we have $K_s = 13.1072$ and $K_b = 65.536$. These parameters will be used throughout the memo.

A suggested value for the false alarm probability is $P_{FA} = 10^{-3}$, which will be used for the remainder of this paper, while a possible maximum target value for the missed detection probability is $P_{MD} = 10^{-6}$. Also, all P_{MD} results will be plotted as a function of the detection time T_d, although a target value for the number of symbols $N_{\text{sym}} = 255$ has been suggested.

Finally, for subsequent notational simplicity, we will define the following standard deviation [2] type quantities:

$$\sigma_b \triangleq \begin{cases} \sqrt{\dfrac{4K_b}{GN_{\text{sym}}}}, & \text{multiple UDC, single phase case} \\ \sqrt{\dfrac{4K_b}{N_{\text{spp}}}}, & \text{single UDC, multiple phase case} \end{cases}, \tag{45}$$

$$\sigma_{s,b} \triangleq \begin{cases} \sqrt{\dfrac{K_s + 4K_b}{GN_{\text{sym}}}}, & \text{multiple UDC, single phase case} \\ \sqrt{\dfrac{K_s + 4K_b}{N_{\text{spp}}}}, & \text{single UDC, multiple phase case} \end{cases}. \tag{46}$$

These quantities will be used throughout the memo.

A. Single UDC, Single Phase Case

Here, we have $G = 1$, and so for this degenerate case, the multiple UDC, single phase and single UDC, multiple phase systems are identical. Thus, from (9) and (19), we get

$$\mathbf{g} = \mathrm{g} = \mathrm{g}_0 = \mathrm{D}_0 \,.$$

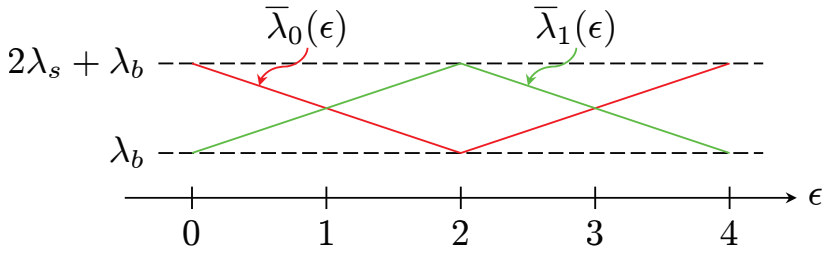

Figure 5. Plots of $\overline{\lambda}_0(\epsilon)$ and $\overline{\lambda}_1(\epsilon)$ from (48) as a function of ϵ for $0 \leq \epsilon < 4$.

Hence, from (20), it follows that we have

$$\mathrm{g} \,|\, \epsilon \sim \mathcal{N}\left(\left(\overline{\lambda}_0(\epsilon) - \overline{\lambda}_1(\epsilon)\right) T_c, \frac{\left(\overline{\lambda}_0(\epsilon) + \overline{\lambda}_1(\epsilon)\right) T_c}{N_{\mathrm{sym}}} \right) , \tag{47}$$

where we have $T_c = 2T_s$ from (6). From (11) and (4), it can be shown that we have the following for $\overline{\lambda}_0(\epsilon)$ and $\overline{\lambda}_1(\epsilon)$, respectively, in the case of telemetry being present:

$$\left.\begin{array}{rcl} \overline{\lambda}_0(\epsilon) & = & \lambda_s \left|\epsilon - 2\right| + \lambda_b \\ \overline{\lambda}_1(\epsilon) & = & \lambda_s \left(2 - \left|\epsilon - 2\right|\right) + \lambda_b \end{array}\right\} \; 0 \leq \epsilon < 4 \, . \tag{48}$$

Plots of $\overline{\lambda}_0(\epsilon)$ and $\overline{\lambda}_1(\epsilon)$ from (48) as a function of ϵ are shown in Fig. 5. As can be seen, $\overline{\lambda}_0(\epsilon)$ and $\overline{\lambda}_1(\epsilon)$ sum up to a constant value of $2\left(\lambda_s + \lambda_b\right)$ and $\overline{\lambda}_1(\epsilon)$ is simply a cyclically shifted version of $\overline{\lambda}_0(\epsilon)$ (as $\overline{\lambda}_0(\epsilon)$ and $\overline{\lambda}_1(\epsilon)$ are periodic functions of ϵ with period 4 here).

From (48), we have the following:

$$\begin{array}{rcl} \left(\overline{\lambda}_0(\epsilon) - \overline{\lambda}_1(\epsilon)\right) T_c & = & \left\{ \begin{array}{ll} 0 \, , & \text{under } H_0 \\ K_s \left(\left|\epsilon - 2\right| - 1\right) \, , & \text{under } H_1 \end{array} \right. , \\ \dfrac{\left(\overline{\lambda}_0(\epsilon) + \overline{\lambda}_1(\epsilon)\right) T_c}{N_{\mathrm{sym}}} & = & \left\{ \begin{array}{ll} \frac{4K_b}{N_{\mathrm{sym}}} \, , & \text{under } H_0 \\ \frac{K_s + 4K_b}{N_{\mathrm{sym}}} \, , & \text{under } H_1 \end{array} \right. . \end{array}$$

Thus, from (47) and (1), we have

$$f_{\mathrm{g} \,|\, H_0}(g) = \frac{1}{\sqrt{\frac{4K_b}{N_{\mathrm{sym}}}}} \phi\left(\frac{g}{\sqrt{\frac{4K_b}{N_{\mathrm{sym}}}}} \right) , \tag{49}$$

$$f_{\mathrm{g} \,|\, H_1, \epsilon}(g \,|\, \epsilon) = \frac{1}{\sqrt{\frac{K_s + 4K_b}{N_{\mathrm{sym}}}}} \phi\left(\frac{g - K_s \left(\left|\epsilon - 2\right| - 1\right)}{\sqrt{\frac{K_s + 4K_b}{N_{\mathrm{sym}}}}} \right) , \; 0 \leq \epsilon < 4 \, . \tag{50}$$

Substituting (50) into (35), it can be shown that we have the following after some algebraic manipulation:

$$f_{\mathrm{g} \,|\, H_1}(g) = \frac{1}{2K_s} \left[\Phi\left(\frac{g + K_s}{\sqrt{\frac{K_s + 4K_b}{N_{\mathrm{sym}}}}} \right) - \Phi\left(\frac{g - K_s}{\sqrt{\frac{K_s + 4K_b}{N_{\mathrm{sym}}}}} \right) \right] . \tag{51}$$

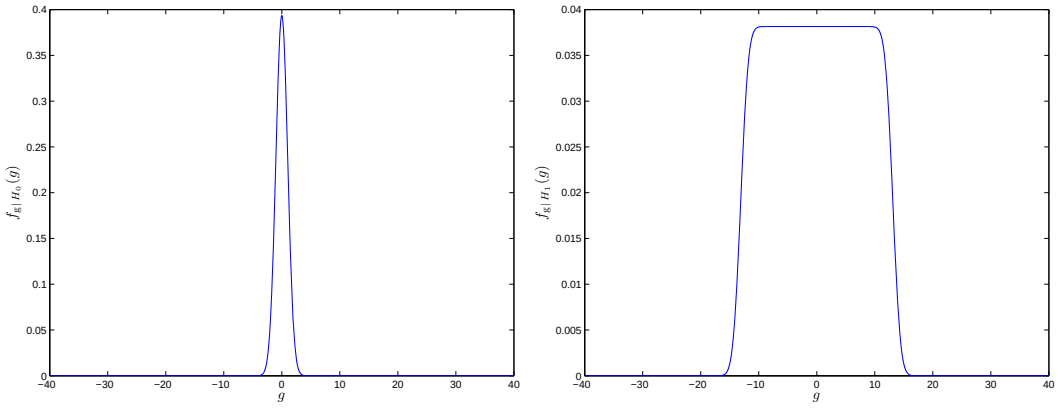

(a) (b)

Figure 6. Single UDC, single phase pdf plots: (a) $f_{g\,|\,H_0}(g)$ and (b) $f_{g\,|\,H_1}(g)$. (Here, $K_s = 13.1072$, $K_b = 65.536$, and $N_{\rm sym} = 255$.)

Using (45) and (46) in (49) and (51), yields

$$f_{g\,|\,H_0}(g) = \frac{1}{\sigma_b}\phi\left(\frac{g}{\sigma_b}\right), \tag{52}$$

$$f_{g\,|\,H_1}(g) = \frac{1}{2K_s}\left[\Phi\left(\frac{g+K_s}{\sigma_{s,b}}\right) - \Phi\left(\frac{g-K_s}{\sigma_{s,b}}\right)\right]. \tag{53}$$

Plots of the pdfs $f_{g\,|\,H_0}(g)$ and $f_{g\,|\,H_1}(g)$ from (52) and (53) are shown in Fig. 6(a) and (b), respectively, for the parameters mentioned at the beginning of this section. As can be seen from Fig. 6(b), in the presence of telemetry, the UDC test statistic g will have zero mean as it does for the case of telemetry being absent, but will have a larger variance due to the presence of signal illumination.

Heuristically, it appears from Fig. 6(b) that $f_{g\,|\,H_1}(g)$ is approximately uniformly distributed over the interval $[-K_s, K_s)$. For the case in which $N_{\rm sym}$ is large, we can show that this will approximately be true. To show this, we first note that as the variance of a normal cdf goes to zero, the cdf will approach a step function [2]. In other words, from (1), it can be shown that we have

$$\lim_{\sigma\to 0}\Phi\left(\frac{x-\mu}{\sigma}\right) = u(x-\mu), \tag{54}$$

where $u(x)$ is the *Heaviside step function* [2] defined as

$$u(x) \triangleq \begin{cases} 0, & x < 0 \\ 1, & x \geq 0 \end{cases}.$$

Now, from (46), it is clear that $\sigma_{s,b} \to 0$ as $N_{\rm sym}$ gets larger. Hence, using (54) in (53), we

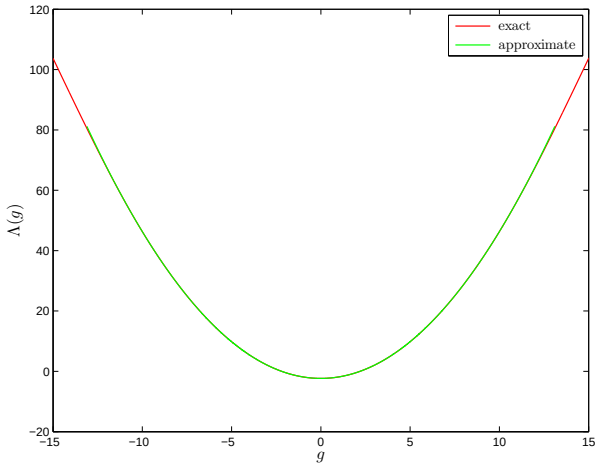

Figure 7. Plot of the exact log likelihood ratio $\Lambda(g)$ along with its approximation in (56) for the single UDC, single phase case ($K_s = 13.1072$, $K_b = 65.536$, and $N_{\text{sym}} = 255$).

get the following approximation for the present hypothesis pdf:

$$f_{\mathrm{g}\,|\,H_1}(g) \approx \frac{1}{2K_s}\left[u(g+K_s) - u(g-K_s)\right] = \begin{cases} 0\,, & g < -K_s \\ \frac{1}{2K_s}\,, & -K_s \le g < K_s \\ 0\,, & g \ge K_s \end{cases} . \tag{55}$$

Thus, g is approximately uniform over the interval $[-K_s, K_s)$, which we will express as $\mathrm{g} \sim \mathcal{U}\,[-K_s, K_s)$.

Continuing further, it can be seen from (52) and (53) that a closed form expression for the log likelihood ratio $\Lambda(g)$ given in (33) does not exist. However, by using the uniform distribution approximation for $f_{\mathrm{g}\,|\,H_1}(g)$ as given in (55), a closed form approximate expression can be obtained. Upon using (55) and (52) with (33), we obtain the following approximation for the log likelihood ratio:

$$\Lambda(g) \approx \begin{cases} \infty\,, & g < -K_s \\ \frac{g^2}{2\sigma_b^2} - \log\left(\frac{2K_s}{\sqrt{2\pi\sigma_b^2}}\right), & -K_s \le g < K_s \\ \infty\,, & g \ge K_s \end{cases} . \tag{56}$$

A plot of the exact log likelihood ratio $\Lambda(g)$ along with its approximation in (56) is shown in Fig. 7 for the above suggested parameters. As can be seen, the approximate log likelihood ratio is a very good fit to the exact expression for $-K_s \le g < K_s$.

To return to the Neyman-Pearson hypothesis test from (36), we will use the log likelihood ratio approximation from (56). Assuming that the threshold value η from (36) is in the region where $\Lambda(g)$ is finite, then from (56), (40), and (38) we have

$$\mathcal{R}_{H_0} = \{g : |g| < r_0\}\,,\ \mathcal{R}_{H_1} = \{g : |g| > r_0\}\,, \tag{57}$$

where r_0 is a threshold value that is a function of the original threshold η. Using (57) and (52) in (37), the false alarm probability P_{FA} can be shown to be

$$P_{FA} = 2\left[1 - \Phi\left(\frac{r_0}{\sigma_b}\right)\right] .$$

Enforcing the constraint that $P_{FA} = \alpha$ as required for the Neyman-Pearson hypothesis test leads to the following for the threshold value r_0:

$$r_0 = \sigma_b \Phi^{-1}\left(1 - \frac{\alpha}{2}\right) , \tag{58}$$

where $\Phi^{-1}(x)$ is the *quantile* function of the standard normal distribution (i.e., the inverse of the standard normal cdf $\Phi(x)$) [2]. In terms of the threshold r_0, the missed detection probability P_{MD} can be expressed as follows using (39), (57), and (53) after some algebraic manipulation:

$$\begin{aligned} P_{MD} \;=\; & \left[\Phi\left(\frac{r_0 + K_s}{\sigma_{s,b}}\right) + \Phi\left(\frac{r_0 - K_s}{\sigma_{s,b}}\right) - 1\right] + \frac{r_0}{K_s}\left[\Phi\left(\frac{r_0 + K_s}{\sigma_{s,b}}\right) - \Phi\left(\frac{r_0 - K_s}{\sigma_{s,b}}\right)\right] \\ & + \frac{\sigma_{s,b}}{K_s}\left[\phi\left(\frac{r_0 + K_s}{\sigma_{s,b}}\right) - \phi\left(\frac{r_0 - K_s}{\sigma_{s,b}}\right)\right] \end{aligned} . \tag{59}$$

This results follows from exploiting the following properties of the $\phi(x)$ and $\Phi(x)$ functions [2]:

$$\phi(-x) = \phi(x) \;,\; \Phi(-x) = 1 - \Phi(x) \;,\; \int \Phi(x)\, dx = x\Phi(x) + \phi(x) \;.$$

Using the threshold value for r_0 from (58) in (59), we then have an expression for P_{MD} as a function of K_b, K_s, N_{sym}, and α. A plot of the missed detection probability P_{MD} as a function of the detection time T_d for the parameters mentioned at the beginning of this section is shown in Fig. 8. As can be seen, the probability of missed detection is excessively large here and well above the maximum target value of 10^{-6}. This shows that for this possible operating point that a single UDC, single phase system will not be sufficient for uplink signal detection.

B. Dual UDC, Single Phase Case

Here, we have $G = 2$, and so from (23), (24), and (25), we get

$$\mathbf{D} \,|\, \epsilon \sim \mathcal{N}_2\left(\boldsymbol{\mu}_{\mathbf{D}|\epsilon}, \boldsymbol{\Sigma}_{\mathbf{D}|\epsilon}\right) , \tag{60}$$

where we have

$$\boldsymbol{\mu}_{\mathbf{D}|\epsilon} \;=\; \begin{bmatrix} \left(\overline{\lambda}_0(\epsilon) - \overline{\lambda}_2(\epsilon)\right) T_c \\ \left(\overline{\lambda}_1(\epsilon) - \overline{\lambda}_3(\epsilon)\right) T_c \end{bmatrix} , \tag{61}$$

$$\boldsymbol{\Sigma}_{\mathbf{D}|\epsilon} \;=\; \begin{bmatrix} \frac{\left(\overline{\lambda}_0(\epsilon) + \overline{\lambda}_2(\epsilon)\right) T_c}{N_{\text{sym}}} & 0 \\ 0 & \frac{\left(\overline{\lambda}_1(\epsilon) + \overline{\lambda}_3(\epsilon)\right) T_c}{N_{\text{sym}}} \end{bmatrix} . \tag{62}$$

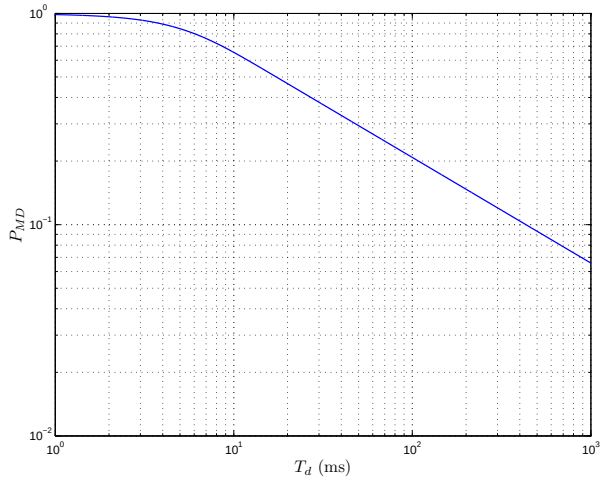

Figure 8. Plot of the missed detection probability P_{MD} as a function of the detection time T_d for the single UDC, single phase case ($K_s = 13.1072$, $K_b = 65.536$).

Here, $T_c = T_s$ from (6). To obtain the symbol timing offset dependent arrival rates $\left\{\overline{\lambda}_r(\epsilon)\right\}_{r=0}^{3}$, note that from (11) and (4) that we have $\overline{\lambda}_r(\epsilon) = \lambda_b$ for all r under H_0. Under H_1, it can be shown that we have the following:

$$
\begin{aligned}
\overline{\lambda}_0(\epsilon) &= \begin{cases} \lambda_s 2\,(1-\epsilon) + \lambda_b\,, & 0 \le \epsilon < 1 \\ \lambda_b\,, & 1 \le \epsilon < 2 \\ \lambda_s 2\,(\epsilon - 2) + \lambda_b\,, & 2 \le \epsilon < 3 \\ 2\lambda_s + \lambda_b\,, & 3 \le \epsilon < 4 \end{cases}, \\
\overline{\lambda}_1(\epsilon) &= \begin{cases} 2\lambda_s + \lambda_b\,, & 0 \le \epsilon < 1 \\ \lambda_s 2\,(2-\epsilon) + \lambda_b\,, & 1 \le \epsilon < 2 \\ \lambda_b\,, & 2 \le \epsilon < 3 \\ \lambda_s 2\,(\epsilon - 3) + \lambda_b\,, & 3 \le \epsilon < 4 \end{cases}, \\
\overline{\lambda}_2(\epsilon) &= \begin{cases} \lambda_s 2\epsilon + \lambda_b\,, & 0 \le \epsilon < 1 \\ 2\lambda_s + \lambda_b\,, & 1 \le \epsilon < 2 \\ \lambda_s 2\,(3-\epsilon) + \lambda_b\,, & 2 \le \epsilon < 3 \\ \lambda_b\,, & 3 \le \epsilon < 4 \end{cases}, \\
\overline{\lambda}_3(\epsilon) &= \begin{cases} \lambda_b\,, & 0 \le \epsilon < 1 \\ \lambda_s 2\,(\epsilon - 1) + \lambda_b\,, & 1 \le \epsilon < 2 \\ 2\lambda_s + \lambda_b\,, & 2 \le \epsilon < 3 \\ \lambda_s 2\,(4-\epsilon) + \lambda_b\,, & 3 \le \epsilon < 4 \end{cases}.
\end{aligned}
\tag{63}
$$

Plots of $\left\{\overline{\lambda}_r(\epsilon)\right\}_{r=0}^{3}$ from (63) as a function of ϵ are shown in Fig. 9. Similar to the single UDC case shown in Fig. 5, it can be seen from Fig. 9 that $\overline{\lambda}_{(r+1) \bmod 4}(\epsilon)$ is simply a cyclically shifted version of $\overline{\lambda}_r(\epsilon)$ for $0 \le r \le 3$.

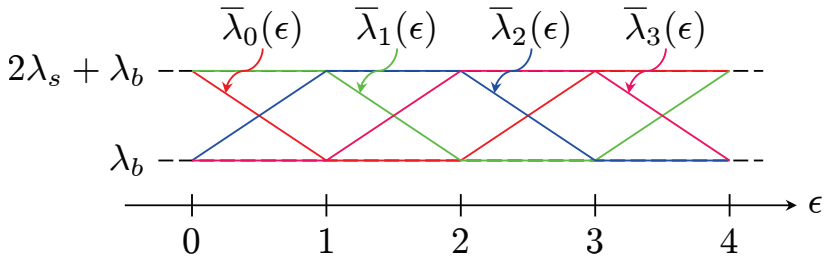

Figure 9. Plots of $\left\{\overline{\lambda}_r(\epsilon)\right\}_{r=0}^{3}$ from (63) as a function of ϵ for $0 \le \epsilon < 4$.

Combining (63), (45), and (46) with (61) and (62) leads to the following:

$$\boldsymbol{\mu}_{\mathbf{D}|\epsilon} = \begin{cases} \begin{bmatrix} 0 \\ 0 \end{bmatrix}, & \text{under } H_0 \\ \begin{bmatrix} \frac{K_s}{2}\overline{\mu}_{\mathrm{D}_0}(\epsilon) \\ \frac{K_s}{2}\overline{\mu}_{\mathrm{D}_1}(\epsilon) \end{bmatrix}, & \text{under } H_1 \end{cases}, \quad \boldsymbol{\Sigma}_{\mathbf{D}|\epsilon} = \begin{cases} \sigma_b^2\mathbf{I}_2\,, & \text{under } H_0 \\ \sigma_{s,b}^2\mathbf{I}_2\,, & \text{under } H_1 \end{cases}, \tag{64}$$

where $\overline{\mu}_{\mathrm{D}_0}(\epsilon)$ and $\overline{\mu}_{\mathrm{D}_1}(\epsilon)$ are defined as

$$\begin{aligned} \overline{\mu}_{\mathrm{D}_0}(\epsilon) &\triangleq \begin{cases} 1-2\epsilon\,, & 0 \le \epsilon < 1 \\ -1\,, & 1 \le \epsilon < 2 \\ -1+2\,(\epsilon-2)\,, & 2 \le \epsilon < 3 \\ 1\,, & 3 \le \epsilon < 4 \end{cases}, \\ \overline{\mu}_{\mathrm{D}_1}(\epsilon) &\triangleq \begin{cases} 1\,, & 0 \le \epsilon < 1 \\ 1-2\,(\epsilon-1)\,, & 1 \le \epsilon < 2 \\ -1\,, & 2 \le \epsilon < 3 \\ -1+2\,(\epsilon-3)\,, & 3 \le \epsilon < 4 \end{cases}. \end{aligned} \tag{65}$$

Using (64) in (60), it follows that under H_0, we have

$$f_{\mathbf{D}\,|\,H_0}(\boldsymbol{D}) = f_{\mathrm{D}_0,\mathrm{D}_1\,|\,H_0}(D_0, D_1) = \frac{1}{\sigma_b^2}\phi\left(\frac{D_0}{\sigma_b}\right)\phi\left(\frac{D_1}{\sigma_b}\right), \tag{66}$$

whereas under H_1, we have

$$f_{\mathbf{D}\,|\,H_1,\varepsilon}(\boldsymbol{D}\,|\,\epsilon) = f_{\mathrm{D}_0,\mathrm{D}_1\,|\,H_1,\varepsilon}(D_0, D_1\,|\,\epsilon) = \frac{1}{\sigma_{s,b}^2}\phi\left(\frac{D_0 - \frac{K_s}{2}\overline{\mu}_{\mathrm{D}_0}(\epsilon)}{\sigma_{s,b}}\right)\phi\left(\frac{D_1 - \frac{K_s}{2}\overline{\mu}_{\mathrm{D}_1}(\epsilon)}{\sigma_{s,b}}\right). \tag{67}$$

Substituting (67) and (65) into (35), it can be shown that we have the following after

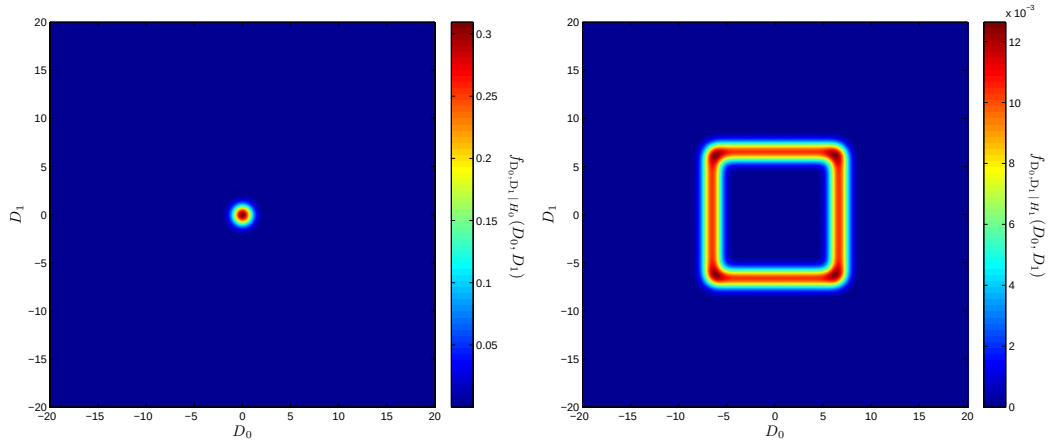

(a) (b)

Figure 10. Dual UDC, single phase pdf plots: (a) $f_{\mathrm{D}_0,\mathrm{D}_1 \mid H_0}(D_0, D_1)$ and (b) $f_{\mathrm{D}_0,\mathrm{D}_1 \mid H_1}(D_0, D_1)$. (Here, $K_s = 13.1072$, $K_b = 65.536$, and $N_{\mathrm{sym}} = 255$.)

much algebraic manipulation:

$$
\begin{aligned}
f_{\mathrm{D}_0,\mathrm{D}_1 \mid H_1}(D_0, D_1) \quad = \quad & \frac{1}{2}\left\{\frac{1}{K_s}\left[\Phi\left(\frac{D_0 + \frac{K_s}{2}}{\sigma_{s,b}}\right) - \Phi\left(\frac{D_0 - \frac{K_s}{2}}{\sigma_{s,b}}\right)\right]\right. \\
& \times \frac{1}{2}\left[\frac{1}{\sigma_{s,b}}\phi\left(\frac{D_1 + \frac{K_s}{2}}{\sigma_{s,b}}\right) + \frac{1}{\sigma_{s,b}}\phi\left(\frac{D_1 - \frac{K_s}{2}}{\sigma_{s,b}}\right)\right] \\
& + \frac{1}{K_s}\left[\Phi\left(\frac{D_1 + \frac{K_s}{2}}{\sigma_{s,b}}\right) - \Phi\left(\frac{D_1 - \frac{K_s}{2}}{\sigma_{s,b}}\right)\right] \\
& \left. \times \frac{1}{2}\left[\frac{1}{\sigma_{s,b}}\phi\left(\frac{D_0 + \frac{K_s}{2}}{\sigma_{s,b}}\right) + \frac{1}{\sigma_{s,b}}\phi\left(\frac{D_0 - \frac{K_s}{2}}{\sigma_{s,b}}\right)\right]\right\}
\end{aligned}
\qquad . \qquad (68)
$$

Plots of the pdfs $f_{\mathrm{D}_0,\mathrm{D}_1 \mid H_0}(D_0, D_1)$ and $f_{\mathrm{D}_0,\mathrm{D}_1 \mid H_1}(D_0, D_1)$ from (66) and (68) are shown in Fig. 10(a) and (b), respectively, for the parameters stated at the beginning of this section. As can be seen, $f_{\mathrm{D}_0,\mathrm{D}_1 \mid H_0}(D_0, D_1)$ is concentrated near the origin, whereas $f_{\mathrm{D}_0,\mathrm{D}_1 \mid H_1}(D_0, D_1)$ is concentrated along an L^∞ norm circle of radius $\frac{K_s}{2}$ [8].

A plot of the log likelihood ratio $\Lambda(D_0, D_1)$ given by (33), (68), and (66) is shown in Fig. 11 for the above mentioned parameters. As can be seen, the behavior of the log likelihood ratio is difficult to deduce and there does not appear to be a tractable form for the decision regions $\mathcal{R}_{H_0}$ and $\mathcal{R}_{H_1}$ from (40) and (38), respectively, for a given threshold value η.

From the view of the present hypothesis pdf $f_{\mathrm{D}_0,\mathrm{D}_1 \mid H_1}(D_0, D_1)$ shown in Fig. 10(b) as well as that of the log likelihood ratio $\Lambda(D_0, D_1)$ for small arguments given in Fig. 11, it appears as though an approximate log likelihood ratio decision based rule is as follows:

$$
||\boldsymbol{D}||_\infty = \max\{|D_0|, |D_1|\} \underset{H_0}{\overset{H_1}{\gtrless}} \eta\,, \qquad (69)
$$

where $||\boldsymbol{x}||_\infty$ denotes the L^∞ norm of a vector $\boldsymbol{x}$ [8].

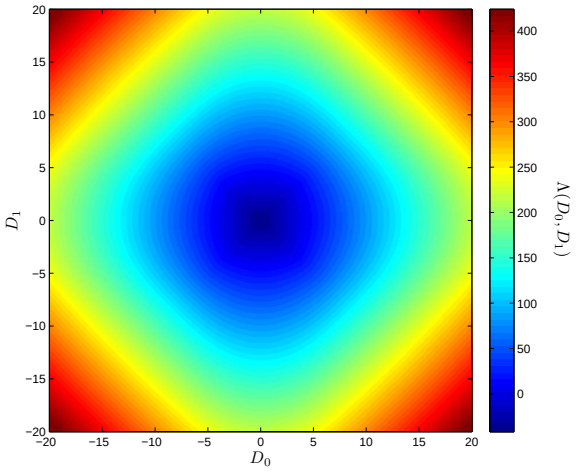

Figure 11. Plot of the log likelihood ratio $\Lambda(D_0, D_1)$ for the dual UDC, single phase case ($K_s = 13.1072$, $K_b = 65.536$, and $N_{\rm sym} = 255$).

C. Single UDC, Dual Phase Case

Once again, we have $G = 2$, and so from (30), (31), and (32), we have the following:

$$\mathbf{g} \,|\, \epsilon \sim \mathcal{N}_2\Big(\boldsymbol{\mu}_{\mathbf{g}|\epsilon}, \boldsymbol{\Sigma}_{\mathbf{g}|\epsilon}\Big) \,, \tag{70}$$

where we have

$$\begin{aligned} \boldsymbol{\mu}_{\mathbf{g}|\epsilon} &= \begin{bmatrix} \big(\overline{\lambda}_0(\epsilon) - \overline{\lambda}_2(\epsilon)\big)\, T_c + \big(\overline{\lambda}_1(\epsilon) - \overline{\lambda}_3(\epsilon)\big)\, T_c \\ -\big(\overline{\lambda}_0(\epsilon) - \overline{\lambda}_2(\epsilon)\big)\, T_c + \big(\overline{\lambda}_1(\epsilon) - \overline{\lambda}_3(\epsilon)\big)\, T_c \end{bmatrix} , \\ \boldsymbol{\Sigma}_{\mathbf{g}|\epsilon} &= \left[\frac{\big(\overline{\lambda}_0(\epsilon) + \overline{\lambda}_2(\epsilon)\big)\, T_c}{N_{\rm spp}} + \frac{\big(\overline{\lambda}_1(\epsilon) + \overline{\lambda}_3(\epsilon)\big)\, T_c}{N_{\rm spp}} \right] \mathbf{I}_2 \,. \end{aligned}$$

As before, we have $T_c = T_s$ here. Using (63), along with (45) and (46), we get

$$\boldsymbol{\mu}_{\mathbf{g}|\epsilon} = \begin{cases} \begin{bmatrix} 0 \\ 0 \end{bmatrix} , & \text{under } H_0 \\ \begin{bmatrix} K_s \overline{\mu}_{\mathrm{g}_0}(\epsilon) \\ K_s \overline{\mu}_{\mathrm{g}_1}(\epsilon) \end{bmatrix} , & \text{under } H_1 \end{cases} , \; \boldsymbol{\Sigma}_{\mathbf{g}|\epsilon} = \begin{cases} \sigma_b^2 \mathbf{I}_2 \,, & \text{under } H_0 \\ \sigma_{s,b}^2 \mathbf{I}_2 \,, & \text{under } H_1 \end{cases} , \tag{71}$$

where $\overline{\mu}_{\mathrm{g}_0}(\epsilon)$ and $\overline{\mu}_{\mathrm{g}_1}(\epsilon)$ are defined as

$$\overline{\mu}_{\mathrm{g}_0}(\epsilon) \triangleq \begin{cases} 1 - \epsilon \,, & 0 \le \epsilon < 1 \\ 1 - \epsilon \,, & 1 \le \epsilon < 2 \\ \epsilon - 3 \,, & 2 \le \epsilon < 3 \\ \epsilon - 3 \,, & 3 \le \epsilon < 4 \end{cases} , \; \overline{\mu}_{\mathrm{g}_1}(\epsilon) \triangleq \begin{cases} \epsilon \,, & 0 \le \epsilon < 1 \\ 2 - \epsilon \,, & 1 \le \epsilon < 2 \\ 2 - \epsilon \,, & 2 \le \epsilon < 3 \\ \epsilon - 4 \,, & 3 \le \epsilon < 4 \end{cases} . \tag{72}$$

Using (71) in (70), it follows that under H_0, we have

$$f_{\mathbf{g}\,|\,H_0}(\boldsymbol{g}) = f_{\mathrm{g}_0,\mathrm{g}_1\,|\,H_0}(g_0, g_1) = \frac{1}{\sigma_b^2} \phi\left(\frac{g_0}{\sigma_b}\right) \phi\left(\frac{g_1}{\sigma_b}\right) , \tag{73}$$

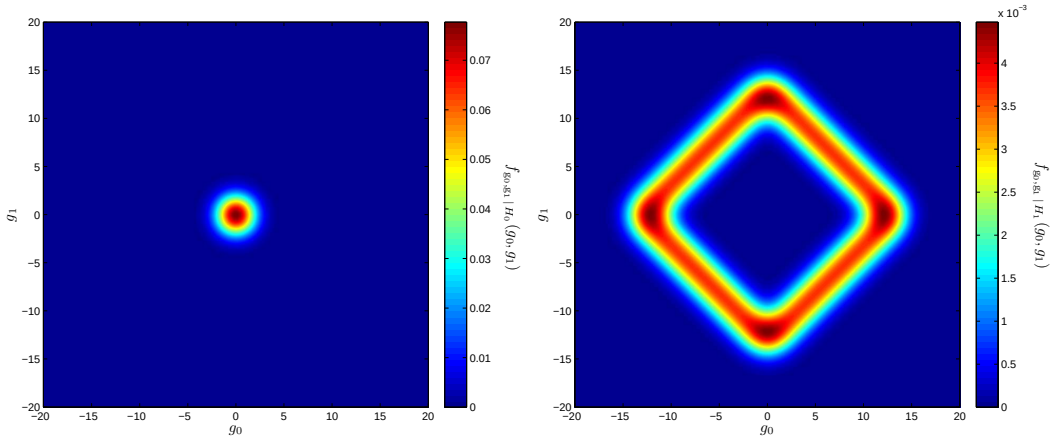

(a) (b)

Figure 12. Single UDC, dual phase pdf plots: (a) $f_{\mathrm{g}_0,\mathrm{g}_1\,|\,H_0}(g_0,g_1)$ and (b) $f_{\mathrm{g}_0,\mathrm{g}_1\,|\,H_1}(g_0,g_1)$. (Here, $K_s=13.1072$, $K_b=65.536$, and $N_{\mathrm{spp}}=128$.)

whereas under H_1, we have

$$f_{\mathbf{g}\,|\,H_1,\boldsymbol{\varepsilon}}(\boldsymbol{g}\,|\,\epsilon)=f_{\mathrm{g}_0,\mathrm{g}_1\,|\,H_1,\boldsymbol{\varepsilon}}(g_0,g_1\,|\,\epsilon)=\frac{1}{\sigma_{s,b}^2}\phi\!\left(\frac{g_0-K_s\overline{\mu}_{\mathrm{g}_0}(\epsilon)}{\sigma_{s,b}}\right)\phi\!\left(\frac{g_1-K_s\overline{\mu}_{\mathrm{g}_1}(\epsilon)}{\sigma_{s,b}}\right). \quad (74)$$

Substituting (74) and (72) into (35), it can be shown that we have the following after much algebraic manipulation:

$$\begin{aligned}
f_{\mathrm{g}_0,\mathrm{g}_1\,|\,H_1}(g_0,g_1) \;=\; & \frac{1}{2}\left\{\frac{1}{K_s\sqrt{2}}\left[\Phi\!\left(\frac{\left(\frac{g_0+g_1}{\sqrt{2}}\right)+\frac{K_s}{\sqrt{2}}}{\sigma_{s,b}}\right)-\Phi\!\left(\frac{\left(\frac{g_0+g_1}{\sqrt{2}}\right)-\frac{K_s}{\sqrt{2}}}{\sigma_{s,b}}\right)\right]\right.\\
& \times\frac{1}{2}\left[\frac{1}{\sigma_{s,b}}\phi\!\left(\frac{\left(\frac{g_0-g_1}{\sqrt{2}}\right)+\frac{K_s}{\sqrt{2}}}{\sigma_{s,b}}\right)+\frac{1}{\sigma_{s,b}}\phi\!\left(\frac{\left(\frac{g_0-g_1}{\sqrt{2}}\right)-\frac{K_s}{\sqrt{2}}}{\sigma_{s,b}}\right)\right]\\
& +\frac{1}{K_s\sqrt{2}}\left[\Phi\!\left(\frac{\left(\frac{g_0-g_1}{\sqrt{2}}\right)+\frac{K_s}{\sqrt{2}}}{\sigma_{s,b}}\right)-\Phi\!\left(\frac{\left(\frac{g_0-g_1}{\sqrt{2}}\right)-\frac{K_s}{\sqrt{2}}}{\sigma_{s,b}}\right)\right]\\
& \left.\times\frac{1}{2}\left[\frac{1}{\sigma_{s,b}}\phi\!\left(\frac{\left(\frac{g_0+g_1}{\sqrt{2}}\right)+\frac{K_s}{\sqrt{2}}}{\sigma_{s,b}}\right)+\frac{1}{\sigma_{s,b}}\phi\!\left(\frac{\left(\frac{g_0+g_1}{\sqrt{2}}\right)-\frac{K_s}{\sqrt{2}}}{\sigma_{s,b}}\right)\right]\right\}.
\end{aligned} \quad (75)$$

Plots of the pdfs $f_{\mathrm{g}_0,\mathrm{g}_1\,|\,H_0}(g_0,g_1)$ and $f_{\mathrm{g}_0,\mathrm{g}_1\,|\,H_1}(g_0,g_1)$ from (73) and (75) are shown in Fig. 12(a) and (b), respectively, for the parameters stated at the beginning of this section. In order make the detection time approximately commensurate between the single UDC, dual phase case and the dual UDC, single phase case, we have opted to used $N_{\mathrm{spp}}=\left\lceil\frac{255}{2}\right\rceil=128$. As can be seen, $f_{\mathrm{g}_0,\mathrm{g}_1\,|\,H_0}(g_0,g_1)$ is concentrated near the origin, whereas $f_{\mathrm{g}_0,\mathrm{g}_1\,|\,H_1}(D_0,D_1)$ is concentrated along an L^1 norm circle of radius K_s [8].

A plot of the log likelihood ratio $\Lambda(g_0,g_1)$ given by (33), (75), and (73) is shown in Fig. 13 for the above mentioned parameters. As before with the dual UDC, single phase case, it

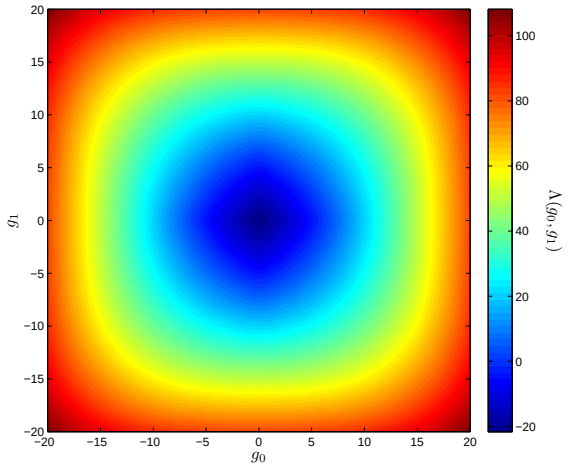

Figure 13. Plot of the log likelihood ratio $\Lambda(g_0, g_1)$ for the single UDC, dual phase case ($K_s = 13.1072$, $K_b = 65.536$, and $N_{\text{spp}} = 128$).

can be seen that the behavior of the log likelihood ratio is not easily deduced and there does not appear to be a tractable form for the decision regions $\mathcal{R}_{H_0}$ and $\mathcal{R}_{H_1}$ from (40) and (38), respectively, for a given threshold value η.

From the view of the present hypothesis pdf $f_{\mathrm{g}_0,\mathrm{g}_1 \,|\, H_1}(g_0, g_1)$ shown in Fig. 12(b) as well as that of the log likelihood ratio $\Lambda(g_0, g_1)$ for small arguments given in Fig. 13, it appears as though an approximate log likelihood ratio decision based rule is as follows:

$$||\boldsymbol{g}||_1 = |g_0| + |g_1| \underset{H_0}{\overset{H_1}{\gtrless}} \eta \,, \tag{76}$$

where $||\boldsymbol{x}||_1$ denotes the L^1 norm of a vector $\boldsymbol{x}$ [8].

VI. Worst Case Scenario Symbol Timing Offset Hypothesis Test Detection Analysis

Perhaps the main problem with assessing the performance of the unconditional Neyman-Pearson hypothesis test is that determining the respective likelihood decision regions $\mathcal{R}_{H_0}$ and $\mathcal{R}_{H_1}$ from (40) and (38) is often very difficult, as evidenced for both the dual UDC, single phase system in Sec. V-B as well as the single UDC, dual phase system in Sec. V-C. This, in turn, makes enforcing the false alarm probability constraint and calculating the resulting probability of missed detection intractable.

One way to circumvent this problem is to derive the Neyman-Pearson hypothesis test conditioned on a specific symbol timing offset value, as described in Sec. IV-A. For example, one possible value to consider which is of practical significance is a worst case scenario (WCS) symbol timing offset, in which the offset is exactly in between two timing phases. From the definition of the chip interval T_c in (6), it is clear that the following symbol timing offsets represent WCS values:

$$\epsilon_{\text{WCS}} = \left(\frac{M+P}{2G}\right) k + \left(\frac{M+P}{4G}\right) \,, \; 0 \leq k \leq (2G) - 1 \,.$$

Without loss of generality, we can choose the first WCS offset, corresponding to $k = 0$. For the case of $M = P = 2$ which we will focus on here, this then becomes $\epsilon_{\text{WCS}} = \frac{1}{G}$.

From (24), (25), (31), and (32), it is clear that the characteristics of the test statistics for both the multiple UDC, single phase and single UDC, multiple phase systems depend on the values of $\left(\overline{\lambda}_k(\epsilon) - \overline{\lambda}_{G+k}(\epsilon)\right)$ and $\left(\overline{\lambda}_k(\epsilon) + \overline{\lambda}_{G+k}(\epsilon)\right)$ for $0 \leq k \leq G-1$. Regardless of the value of ϵ, under H_0, we have $\left(\overline{\lambda}_k(\epsilon) - \overline{\lambda}_{G+k}(\epsilon)\right) = 0$ and $\left(\overline{\lambda}_k(\epsilon) + \overline{\lambda}_{G+k}(\epsilon)\right) = 2\lambda_b$ for all k. For the special case of $\epsilon_{\text{WCS}} = \frac{1}{G}$, it can be show that under H_1, we have

$$\overline{\lambda}_k(\epsilon_{\text{WCS}}) - \overline{\lambda}_{G+k}(\epsilon_{\text{WCS}}) = \begin{cases} 0\,, & k = 0 \\ 2\lambda_s\,, & 1 \leq k \leq G-1 \end{cases}, \tag{77}$$

$$\overline{\lambda}_k(\epsilon_{\text{WCS}}) + \overline{\lambda}_{G+k}(\epsilon_{\text{WCS}}) = 2\left(\lambda_s + \lambda_b\right) = 2\lambda_s + 2\lambda_b \;\; \forall \;\; 0 \leq k \leq G-1\,, \tag{78}$$

Coupled with the fact that $T_c = \frac{2T_s}{G}$ here, we can use (77) and (78) to simplify the UDC test statistics and derive and assess the performance of the Neyman-Pearson hypothesis test for a WCS symbol timing offset.

A. Multiple UDC, Single Phase Case

Combining (77) and (78) with (23), (24), (25), and (2), it can be shown that we have

$$f_{\mathbf{D}\,|\,H_0}(\boldsymbol{D}) = \frac{1}{(2\pi)^{\frac{G}{2}}\left(\det\left(\boldsymbol{\Sigma}_{\mathbf{D}|H_0}\right)\right)^{\frac{1}{2}}} e^{-\frac{1}{2}\left(\boldsymbol{D}-\boldsymbol{\mu}_{\mathbf{D}|H_0}\right)^T \boldsymbol{\Sigma}^{-1}_{\mathbf{D}|H_0}\left(\boldsymbol{D}-\boldsymbol{\mu}_{\mathbf{D}|H_0}\right)}\,, \tag{79}$$

$$f_{\mathbf{D}\,|\,H_1,\boldsymbol{\varepsilon}}(\boldsymbol{D}\,|\,\epsilon_{\text{WCS}}) = \frac{1}{(2\pi)^{\frac{G}{2}}\left(\det\left(\boldsymbol{\Sigma}_{\mathbf{D}|H_1,\boldsymbol{\varepsilon}}\right)\right)^{\frac{1}{2}}} e^{-\frac{1}{2}\left(\boldsymbol{D}-\boldsymbol{\mu}_{\mathbf{D}|H_1,\boldsymbol{\varepsilon}}\right)^T \boldsymbol{\Sigma}^{-1}_{\mathbf{D}|H_1,\boldsymbol{\varepsilon}}\left(\boldsymbol{D}-\boldsymbol{\mu}_{\mathbf{D}|H_1,\boldsymbol{\varepsilon}}\right)}\,, \tag{80}$$

where we have the following upon using (45) and (46):

$$\boldsymbol{\mu}_{\mathbf{D}|H_0} = \mathbf{0}_{G\times 1}\,,\;\; \boldsymbol{\Sigma}_{\mathbf{D}|H_0} = \sigma_b^2 \mathbf{I}_G\,, \tag{81}$$

$$\left[\boldsymbol{\mu}_{\mathbf{D}|H_1,\boldsymbol{\varepsilon}}\right]_k = \begin{cases} 0\,, & k = 0 \\ \frac{K_s}{G}\,, & 1 \leq k \leq G-1 \end{cases}\,,\;\; \boldsymbol{\Sigma}_{\mathbf{D}|H_1,\boldsymbol{\varepsilon}} = \sigma_{s,b}^2 \mathbf{I}_G\,. \tag{82}$$

Upon using (80) and (79) in (41) and (42), we obtain the following likelihood rule after much algebraic manipulation:

$$||\boldsymbol{D} - \boldsymbol{D}_C||^2 \underset{H_0}{\overset{H_1}{\gtrless}} r_0^2\,, \tag{83}$$

where $\boldsymbol{D}_C$ is a $G \times 1$ vector defined as

$$\left[\boldsymbol{D}_C\right]_k \triangleq \begin{cases} 0\,, & k = 0 \\ -\frac{4K_b}{G}\,, & 1 \leq k \leq G-1 \end{cases}\,, \tag{84}$$

and r_0 is a threshold value that is a function of the original threshold η from (42). Also, $||\boldsymbol{x}||$ denotes the *Euclidean* or L^2 norm of a vector $\boldsymbol{x}$ [8]. Note that from (83), the decision rule boundary represents a G-dimensional hypersphere in $\mathbb{R}^G$ [8] with center at $\boldsymbol{D}_C$ and radius r_0. In addition, note that from (84) that the decision boundary center only depends

on the mean background count K_b and the number of UDCs G and does not depend on the number of symbols or the telemetry signal parameters. From (83), the decision regions are as follows:

$$\mathcal{R}_{H_0} \triangleq \left\{ \boldsymbol{D} : ||\boldsymbol{D} - \boldsymbol{D}_C||^2 < r_0^2 \right\}, \mathcal{R}_{H_1} \triangleq \left\{ \boldsymbol{D} : ||\boldsymbol{D} - \boldsymbol{D}_C||^2 > r_0^2 \right\}.$$

To enforce the false alarm probability constraint $P_{FA} = \alpha$, we use (43), (79), and (81) to get

$$P_{FA} = \int_{\mathcal{R}_{H_1}} f_{\mathbf{D}\,|\,H_0}(\boldsymbol{D})\, d\boldsymbol{D} = 1 - \int_{\mathcal{R}_{H_0}} f_{\mathbf{D}\,|\,H_0}(\boldsymbol{D})\, d\boldsymbol{D} = \alpha\,.$$

From this, coupled with (79) and (81), we find

$$1 - \alpha = \int_{\mathcal{R}_{H_0}} \frac{1}{(2\pi)^{\frac{G}{2}}\,\sigma_b^G} e^{-\frac{1}{2\sigma_b^2}||\boldsymbol{D}||^2}\, d\boldsymbol{D}\,. \tag{85}$$

Consider the change of variables $\boldsymbol{x} \triangleq \frac{1}{\sigma_b}\boldsymbol{D}$. Then, we have $\boldsymbol{D} = \sigma_b \boldsymbol{x}$ and so $d\boldsymbol{D} = \sigma_b^G d\boldsymbol{x}$. In addition, we have $||\boldsymbol{D}||^2 = \sigma_b^2\,||\boldsymbol{x}||^2$, and so (85) becomes the following:

$$1 - \alpha = \int_{\mathcal{R}_{\boldsymbol{x}}} \frac{1}{(2\pi)^{\frac{G}{2}}} e^{-\frac{1}{2}||\boldsymbol{x}||^2}\, d\boldsymbol{x}\,, \tag{86}$$

where $\mathcal{R}_{\boldsymbol{x}}$ is the region

$$\mathcal{R}_{\boldsymbol{x}} \triangleq \left\{ \boldsymbol{x} : ||\boldsymbol{x} - \boldsymbol{x}_C||^2 < \frac{r_0^2}{\sigma_b^2} \right\}, \text{ where } \boldsymbol{x}_C \triangleq \frac{1}{\sigma_b}\boldsymbol{D}_C\,. \tag{87}$$

Using the result from the Appendix given in (A-1) with (86) and (87) leads to the following:

$$1 - \alpha = F_{NC\chi^2}\left(\frac{r_0^2}{\sigma_b^2}; G, ||\boldsymbol{x}_C||^2 \right).$$

Inverting this relation to obtain the threshold r_0^2 yields

$$r_0^2 = \sigma_b^2 F^{-1}_{NC\chi^2}\left(1 - \alpha; G, ||\boldsymbol{x}_C||^2\right). \tag{88}$$

To further simplify (88), note that from (87), (84), and (45) that we have

$$||\boldsymbol{x}_C||^2 = \frac{1}{\sigma_b^2}||\boldsymbol{D}_C||^2 = \frac{GN_{\text{sym}}}{4K_b} \cdot \left(-\frac{4K_b}{G}\right)^2 \cdot (G-1) = (4K_b)\,N_{\text{sym}}\left(\frac{G-1}{G}\right).$$

Hence, (88) simplifies to

$$r_0^2 = \left(\frac{4K_b}{GN_{\text{sym}}}\right) F^{-1}_{NC\chi^2}\left(1 - \alpha; G, (4K_b)\,N_{\text{sym}}\left(\frac{G-1}{G}\right)\right). \tag{89}$$

Note that this relation provides for a way to determine the decision threshold r_0^2 to satisfy the false alarm probability constraint $P_{FA} = \alpha$. Assuming that r_0^2 has already been obtained as such, we can calculate the associated missed detection probability P_{MD}.

To compute P_{MD}, we use (44), (80), and (82) to get

$$P_{MD} = \int_{\mathcal{R}_{H_0}} f_{\mathbf{D}\,|\,H_1,\varepsilon}(\boldsymbol{D}\,|\,\epsilon_{\text{WCS}})\, d\boldsymbol{D} = \int_{\mathcal{R}_{H_0}} \frac{1}{(2\pi)^{\frac{G}{2}}\,\sigma_{s,b}^G} e^{-\frac{1}{2\sigma_{s,b}^2}||\boldsymbol{D} - \boldsymbol{\mu}_{\mathbf{D}|H_1,\varepsilon}||^2}\, d\boldsymbol{D}\,. \tag{90}$$

As before, consider the change of variables $\boldsymbol{x} \triangleq \frac{1}{\sigma_{s,b}}\left(\boldsymbol{D} - \boldsymbol{\mu}_{\mathbf{D}|H_1,\boldsymbol{\varepsilon}}\right)$. Then, we have $\boldsymbol{D} = \sigma_{s,b}\boldsymbol{x} + \boldsymbol{\mu}_{\mathbf{D}|H_1,\boldsymbol{\varepsilon}}$ and so $d\boldsymbol{D} = \sigma_{s,b}^G d\boldsymbol{x}$. Substituting this into (90) leads to the following:

$$P_{MD} = \int_{\mathcal{R}_{\boldsymbol{x}}} \frac{1}{(2\pi)^{\frac{G}{2}}} e^{-\frac{1}{2}||\boldsymbol{x}||^2}\, d\boldsymbol{x}\,, \tag{91}$$

where $\mathcal{R}_{\boldsymbol{x}}$ is the region

$$\mathcal{R}_{\boldsymbol{x}} \triangleq \left\{\boldsymbol{x} : ||\boldsymbol{x} - \boldsymbol{x}_C||^2 < \frac{r_0^2}{\sigma_{s,b}^2}\right\}\,, \text{ where } \boldsymbol{x}_C \triangleq \frac{1}{\sigma_{s,b}}\left(\boldsymbol{D}_C - \boldsymbol{\mu}_{\mathbf{D}|H_1,\boldsymbol{\varepsilon}}\right)\,. \tag{92}$$

Exploiting the result from the Appendix given in (A-1) with (91) and (92) leads to the following:

$$P_{MD} = F_{NC\chi^2}\left(\frac{r_0^2}{\sigma_{s,b}^2}; G, ||\boldsymbol{x}_C||^2\right)\,. \tag{93}$$

To further simplify (93), note that from (92), (84), (82), and (46) that we have

$$\begin{aligned} ||\boldsymbol{x}_C||^2 &= \frac{1}{\sigma_{s,b}^2}\left|\left|\boldsymbol{D}_C - \boldsymbol{\mu}_{\mathbf{D}|H_1,\boldsymbol{\varepsilon}}\right|\right|^2 = \frac{GN_{\text{sym}}}{K_s + 4K_b} \cdot \left(-\frac{4K_b}{G} - \frac{K_s}{G}\right)^2 \cdot (G-1)\,, \\ &= (K_s + 4K_b)\, N_{\text{sym}}\left(\frac{G-1}{G}\right)\,. \end{aligned}$$

Hence, (93) simplifies to

$$P_{MD} = F_{NC\chi^2}\left(\frac{r_0^2}{\left[\frac{K_s+4K_b}{GN_{\text{sym}}}\right]}; G, (K_s + 4K_b)\, N_{\text{sym}}\left(\frac{G-1}{G}\right)\right)\,. \tag{94}$$

The relations given in (89) and (94) provide a two-step process by which to assess the performance of the Neyman-Pearson hypothesis test for a multiple UDC, single phase system with a WCS symbol timing offset. First, the decision threshold parameter r_0^2 is computed using (89) to satisfy the false alarm probability constraint $P_{FA} = \alpha$ and then the missed detection probability is calculated as in (94). An alternate, simplified way to determine the performance of the hypothesis test is to define the fictitious parameter β as $\beta \triangleq (GN_{\text{sym}})\, r_0^2$. Then, we can assess the performance of the Neyman-Pearson test as follows here:

$$\begin{aligned} &\text{1) Compute } \beta = (4K_b)\, F_{NC\chi^2}^{-1}\left(1-\alpha; G, (4K_b)\, N_{\text{sym}}\left(\frac{G-1}{G}\right)\right)\,, \\ &\text{2) Calculate } P_{MD} = F_{NC\chi^2}\left(\frac{\beta}{K_s + 4K_b}; G, (K_s + 4K_b)\, N_{\text{sym}}\left(\frac{G-1}{G}\right)\right)\,. \end{aligned} \tag{95}$$

A plot of P_{MD} given by (95) as a function of the detection time $T_d = N_{\text{sym}}T_{\text{sym}}$ is shown in Fig. 14 for the parameters mentioned in Sec. V for various values of G. As can be seen, the performance appears to asymptotically reach a limit as $G \to \infty$. This represents a point of diminishing returns, as increasing G requires both an increase in hardware (in terms of the number of UDCs required), as well as an increase in computational complexity for implementing the hypothesis test specified by (83).

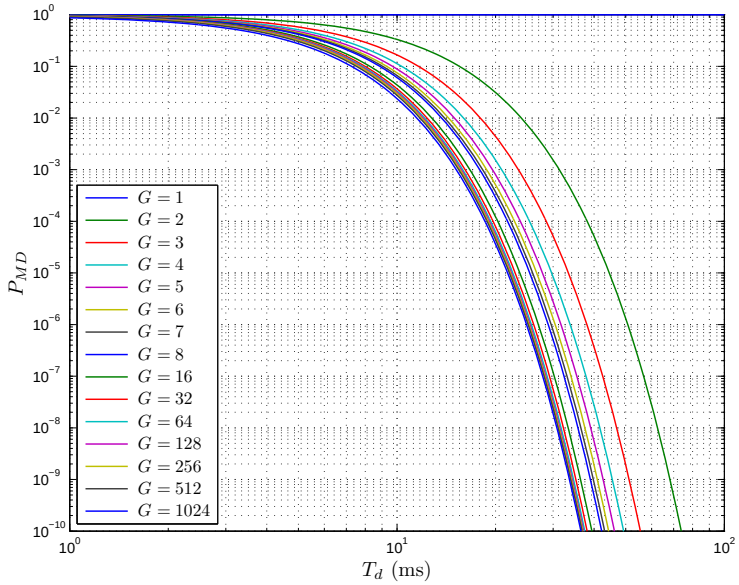

Figure 14. Plot of the missed detection probability P_{MD} given by (95) as a function of the detection time T_d for the multiple UDC, single phase case for a WCS symbol timing offset ($K_s = 13.1072$, $K_b = 65.536$, $P_{FA} = 10^{-3}$).

For the suggested target of $N_{\text{sym}} = 255$ (see the beginning of Sec. V), we have $P_{MD} \approx 1.7628 \times 10^{-9}$ for $G = 2$, which is well below the possible maximum value of 10^{-6}. From this, we can conjecture that a dual UDC, single phase system would suffice for uplink signal detection in this case.

B. Single UDC, Multiple Phase Case

As before, combining (77) and (78) with (30), (31), (32), and (2), it can be shown that we have

$$f_{\mathbf{g}\,|\,H_0}(\boldsymbol{g}) = \frac{1}{(2\pi)^{\frac{G}{2}}\left(\det\left(\boldsymbol{\Sigma}_{\mathbf{g}|H_0}\right)\right)^{\frac{1}{2}}} e^{-\frac{1}{2}(\boldsymbol{g}-\boldsymbol{\mu}_{\mathbf{g}|H_0})^T \boldsymbol{\Sigma}^{-1}_{\mathbf{g}|H_0}(\boldsymbol{D}-\boldsymbol{\mu}_{\mathbf{g}|H_0})}\,, \tag{96}$$

$$f_{\mathbf{g}\,|\,H_1,\varepsilon}(\boldsymbol{g}\,|\,\epsilon_{\text{WCS}}) = \frac{1}{(2\pi)^{\frac{G}{2}}\left(\det\left(\boldsymbol{\Sigma}_{\mathbf{g}|H_1,\varepsilon}\right)\right)^{\frac{1}{2}}} e^{-\frac{1}{2}(\boldsymbol{g}-\boldsymbol{\mu}_{\mathbf{g}|H_1,\varepsilon})^T \boldsymbol{\Sigma}^{-1}_{\mathbf{g}|H_1,\varepsilon}(\boldsymbol{g}-\boldsymbol{\mu}_{\mathbf{g}|H_1,\varepsilon})}\,, \tag{97}$$

where we have the following upon using (45) and (46):

$$\boldsymbol{\mu}_{\mathbf{g}|H_0} = \mathbf{0}_{G\times 1}\,,\ \boldsymbol{\Sigma}_{\mathbf{g}|H_0} = \sigma_b^2 \mathbf{I}_G\,, \tag{98}$$

$$\left[\boldsymbol{\mu}_{\mathbf{g}|H_1,\varepsilon}\right]_k = \frac{K_s}{G}\sum_{r=1}^{G-1}(-1)^{\left\lfloor\frac{r-k}{G}\right\rfloor}\,,\ 0 \le k \le G-1\,,\ \boldsymbol{\Sigma}_{\mathbf{g}|H_1,\varepsilon} = \sigma_{s,b}^2 \mathbf{I}_G\,. \tag{99}$$

It can be shown that we have

$$\sum_{r=1}^{G-1}(-1)^{\left\lfloor\frac{r-k}{G}\right\rfloor} = \begin{cases} G-1\,, & k=0 \\ G-(2k-1)\,, & 1 \le k \le G-1 \end{cases}\,,$$

and so (99) simplifies to

$$\left[\boldsymbol{\mu}_{\mathbf{g}|H_1,\boldsymbol{\varepsilon}}\right]_k = \begin{cases} K_s\left(\frac{G-1}{G}\right), & k=0 \\ K_s\left(\frac{G-(2k-1)}{G}\right), & 1 \le k \le G-1 \end{cases}, \; \boldsymbol{\Sigma}_{\mathbf{g}|H_1,\boldsymbol{\varepsilon}} = \sigma_{s,b}^2 \mathbf{I}_G \,. \tag{100}$$

Upon using (97) and (96) in (41) and (42), we obtain the following likelihood rule after much algebraic manipulation:

$$||\boldsymbol{g} - \boldsymbol{g}_C||^2 \underset{H_0}{\overset{H_1}{\gtrless}} r_0^2 \,, \tag{101}$$

where $\boldsymbol{g}_C$ is a $G \times 1$ vector defined as

$$[\boldsymbol{g}_C]_k \triangleq \begin{cases} -4K_b\left(\frac{G-1}{G}\right), & k=0 \\ -4K_b\left(\frac{G-(2k-1)}{G}\right), & 1 \le k \le G-1 \end{cases}, \tag{102}$$

and r_0 is a threshold value that is a function of the original threshold η from (42). As for the multiple UDC, single phase case, note that from (101), the decision rule boundary represents a G-dimensional hypersphere in $\mathbb{R}^G$ with center at $\boldsymbol{g}_C$ and radius r_0. In addition, note that from (102) that the decision boundary center only depends on the mean background count K_b and the number of UDCs G and does not depend on the number of symbols or the telemetry signal parameters. From (101), the decision regions are as follows:

$$\mathcal{R}_{H_0} \triangleq \left\{\boldsymbol{g} : ||\boldsymbol{g} - \boldsymbol{g}_C||^2 < r_0^2\right\}, \mathcal{R}_{H_1} \triangleq \left\{\boldsymbol{g} : ||\boldsymbol{g} - \boldsymbol{g}_C||^2 > r_0^2\right\}.$$

To enforce the false alarm probability constraint $P_{FA} = \alpha$, we use (43), (96), and (98) to get

$$P_{FA} = \int_{\mathcal{R}_{H_1}} f_{\mathbf{g}\,|\,H_0}(\boldsymbol{g})\; d\boldsymbol{g} = 1 - \int_{\mathcal{R}_{H_0}} f_{\mathbf{g}\,|\,H_0}(\boldsymbol{g})\; d\boldsymbol{g} = \alpha \,.$$

From this, coupled with (96) and (98), we find

$$1 - \alpha = \int_{\mathcal{R}_{H_0}} \frac{1}{(2\pi)^{\frac{G}{2}}\,\sigma_b^G} e^{-\frac{1}{2\sigma_b^2}||\boldsymbol{g}||^2}\, d\boldsymbol{g} \,. \tag{103}$$

Consider the change of variables $\boldsymbol{x} \triangleq \frac{1}{\sigma_b}\boldsymbol{g}$. Then, we have $\boldsymbol{g} = \sigma_b \boldsymbol{x}$ and so $d\boldsymbol{g} = \sigma_b^G d\boldsymbol{x}$. In addition, we have $||\boldsymbol{g}||^2 = \sigma_b^2\,||\boldsymbol{x}||^2$, and so (103) becomes the following:

$$1 - \alpha = \int_{\mathcal{R}_{\boldsymbol{x}}} \frac{1}{(2\pi)^{\frac{G}{2}}} e^{-\frac{1}{2}||\boldsymbol{x}||^2}\, d\boldsymbol{x} \,, \tag{104}$$

where $\mathcal{R}_{\boldsymbol{x}}$ is the region

$$\mathcal{R}_{\boldsymbol{x}} \triangleq \left\{\boldsymbol{x} : ||\boldsymbol{x} - \boldsymbol{x}_C||^2 < \frac{r_0^2}{\sigma_b^2}\right\}, \text{ where } \boldsymbol{x}_C \triangleq \frac{1}{\sigma_b}\boldsymbol{g}_C \,. \tag{105}$$

Using the result from the Appendix given in (A-1) with (104) and (105) leads to the following:

$$1 - \alpha = F_{NC\chi^2}\left(\frac{r_0^2}{\sigma_b^2}; G, ||\boldsymbol{x}_C||^2\right).$$

Inverting this relation to obtain the threshold r_0^2 yields

$$r_0^2 = \sigma_b^2 F_{NC\chi^2}^{-1}\Big(1-\alpha; G, ||\boldsymbol{x}_C||^2\Big)\,. \tag{106}$$

To further simplify (106), note that from (105), (102), and (45) that we have

$$||\boldsymbol{x}_C||^2 = \frac{1}{\sigma_b^2}\,||\boldsymbol{g}_C||^2 = (4K_b)\,N_{\text{spp}}\left[\left(\frac{G-1}{G}\right)^2 + \sum_{k=1}^{G-1}\left(\frac{G-(2k-1)}{G}\right)^2\right]. \tag{107}$$

The expression given in (107) can be simplified upon using the following relations [7]:

$$\sum_{k=1}^{G-1} 1 = G-1\,,\ \sum_{k=1}^{G-1} k = \frac{(G-1)\,G}{2}\,,\ \sum_{k=1}^{G-1} k^2 = \frac{(G-1)\,G\,(2G-1)}{6}\,. \tag{108}$$

Upon using (108) in (107), after some algebraic manipulation, we get

$$||\boldsymbol{x}_C||^2 = (4K_b)\,N_{\text{spp}}\left(\frac{G^2-1}{3G}\right).$$

Hence, (106) simplifies to

$$r_0^2 = \left(\frac{4K_b}{N_{\text{spp}}}\right) F_{NC\chi^2}^{-1}\left(1-\alpha; G, (4K_b)\,N_{\text{spp}}\left(\frac{G^2-1}{3G}\right)\right). \tag{109}$$

Note that this relation provides for a way to determine the decision threshold r_0^2 to satisfy the false alarm probability constraint $P_{FA} = \alpha$. Assuming that r_0^2 has already been obtained as such, we can calculate the associated missed detection probability P_{MD}.

To compute P_{MD}, we use (44), (97), and (100) to get

$$P_{MD} = \int_{\mathcal{R}_{H_0}} f_{\mathbf{g}\,|\,H_1,\varepsilon}(\boldsymbol{g}\,|\,\epsilon_{\text{WCS}})\;d\boldsymbol{g} = \int_{\mathcal{R}_{H_0}} \frac{1}{(2\pi)^{\frac{G}{2}}\,\sigma_{s,b}^G} e^{-\frac{1}{2\sigma_{s,b}^2}||\boldsymbol{g}-\boldsymbol{\mu}_{\mathbf{g}|H_1,\varepsilon}||^2}\,d\boldsymbol{g}\,. \tag{110}$$

As before, consider the change of variables $\boldsymbol{x} \triangleq \frac{1}{\sigma_{s,b}}\Big(\boldsymbol{g}-\boldsymbol{\mu}_{\mathbf{g}|H_1,\varepsilon}\Big)$. Then, we have $\boldsymbol{g} = \sigma_{s,b}\boldsymbol{x} + \boldsymbol{\mu}_{\mathbf{g}|H_1,\varepsilon}$ and so $d\boldsymbol{g} = \sigma_{s,b}^G d\boldsymbol{x}$. Substituting this into (110) leads to the following:

$$P_{MD} = \int_{\mathcal{R}_{\boldsymbol{x}}} \frac{1}{(2\pi)^{\frac{G}{2}}} e^{-\frac{1}{2}||\boldsymbol{x}||^2}\,d\boldsymbol{x}\,, \tag{111}$$

where $\mathcal{R}_{\boldsymbol{x}}$ is the region

$$\mathcal{R}_{\boldsymbol{x}} \triangleq \left\{\boldsymbol{x} : ||\boldsymbol{x}-\boldsymbol{x}_C||^2 < \frac{r_0^2}{\sigma_{s,b}^2}\right\},\ \text{where}\ \boldsymbol{x}_C \triangleq \frac{1}{\sigma_{s,b}}\Big(\boldsymbol{g}_C - \boldsymbol{\mu}_{\mathbf{g}|H_1,\varepsilon}\Big)\,. \tag{112}$$

Exploiting the result from the Appendix given in (A-1) with (111) and (112) leads to the following:

$$P_{MD} = F_{NC\chi^2}\left(\frac{r_0^2}{\sigma_{s,b}^2}; G, ||\boldsymbol{x}_C||^2\right). \tag{113}$$

To further simplify (113), note that from (112), (102), (100), (46), and (108) that we can show that we have

$$||\boldsymbol{x}_C||^2 \;=\; \frac{1}{\sigma_{s,b}^2}\Big|\Big|\boldsymbol{g}_C - \boldsymbol{\mu}_{\mathbf{g}|H_1,\varepsilon}\Big|\Big|^2 = (K_s+4K_b)\,N_{\text{sym}}\left(\frac{G^2-1}{3G}\right).$$

Hence, (113) simplifies to

$$P_{MD} = F_{NC\chi^2}\left(\frac{r_0^2}{\left[\frac{K_s+4K_b}{N_{\text{spp}}}\right]}; G, (K_s+4K_b)\, N_{\text{sym}}\left(\frac{G^2-1}{3G}\right)\right). \tag{114}$$

As with the multiple UDC, single phase system, the relations given in (109) and (114) provide a two-step process by which to assess the performance of the Neyman-Pearson hypothesis test for a single UDC, multiple phase system with a WCS symbol timing offset. First, the decision threshold parameter r_0^2 is computed using (109) to satisfy the false alarm probability constraint $P_{FA} = \alpha$ and then the missed detection probability is calculated as in (114). An alternate, simplified way to determine the performance of the hypothesis test is to define the fictitious parameter β as $\beta \triangleq N_{\text{spp}} r_0^2$. Then, we can assess the performance of the Neyman-Pearson test as follows here:

$$\begin{aligned} &\text{1) Compute } \beta = (4K_b)\, F_{NC\chi^2}^{-1}\left(1-\alpha; G, (4K_b)\, N_{\text{spp}}\left(\frac{G^2-1}{3G}\right)\right), \\ &\text{2) Calculate } P_{MD} = F_{NC\chi^2}\left(\frac{\beta}{K_s+4K_b}; G, (K_s+4K_b)\, N_{\text{spp}}\left(\frac{G^2-1}{3G}\right)\right). \end{aligned} \tag{115}$$

A plot of P_{MD} given by (115) as a function of the detection time $T_d = N_{\text{spp}} G T_{\text{sym}}$ is shown in Fig. 15 for the parameters mentioned in Sec. V for various values of G. As can be seen, the performance appears to asymptotically reach a limit as $G \to \infty$. This represents a point of diminishing returns, as increasing G requires both an increase in hardware (in terms of triggering and storing the count statistics for the number of timing phases required), as well as an increase in computational complexity for implementing the hypothesis test specified by (101).

For the suggested target of $N_{\text{sym}} = 255$, corresponding to a detection time of $T_d = 66.84672$ ms (see Sec. I-C as well as the beginning of Sec. V), we have $P_{MD} \approx 4.9696 \times 10^{-4}$ for $G = 2$, which is well above the possible maximum value of 10^{-6}. From this, we can conjecture that a single UDC, dual phase system would not suffice for uplink signal detection in this case.

VII. Advantages and Disadvantages Between the Multiple UDC, Single Phase and Single UDC, Multiple Phase Detection Systems

As mentioned in Sec. VI-A and VI-B, for the suggested operating point considered here (see the beginning of Sec. V), a dual UDC, single phase system would suffice for uplink signal detection in the case of a WCS symbol timing offset, whereas a single UDC, dual phase system would not. This brings to light some of the trade-offs associated with both the multiple UDC, single phase and single UDC, multiple phase detection schemes.

For a fixed detection time T_d, a multiple UDC, single phase system will exhibit greater detection performance than a single UDC, multiple phase system. Intuitively, the reason

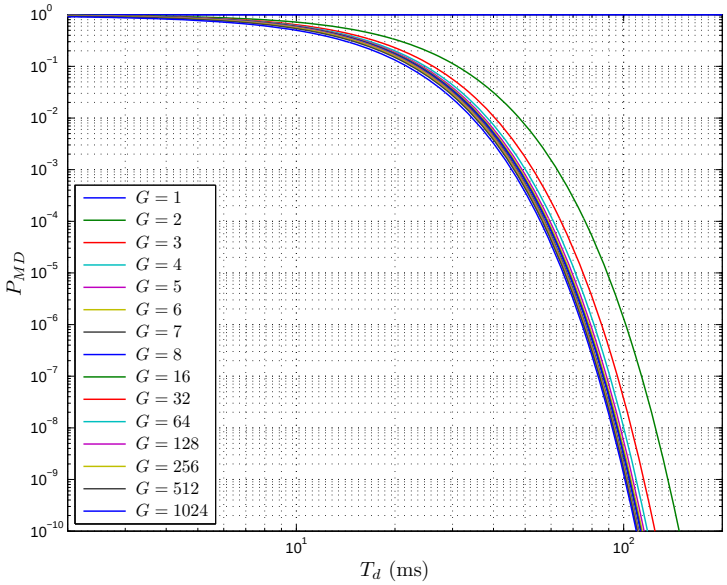

Figure 15. Plot of the missed detection probability P_{MD} given by (115) as a function of the detection time T_d for the single UDC, multiple phase case for a WCS symbol timing offset ($K_s = 13.1072$, $K_b = 65.536$, $P_{FA} = 10^{-3}$).

for this is that the former system has more information available to it to use for signal detection than the latter one. To see this analytically, consider the conditional WCS symbol timing offset detection results derived in Sec. VI. In the case where T_d is fixed, we have $N_{\text{spp}} = \frac{N_{\text{sym}}}{G}$ (see Sec. I-C), and so the performance of the Neyman-Pearson hypothesis test for a WCS symbol timing offset for the single UDC, multiple phase system from (115) becomes

$$\begin{aligned} &1)\ \text{Compute } \beta = (4K_b)\, F^{-1}_{NC\chi^2}\left(1-\alpha; G, (4K_b)\, N_{\text{sym}} \left(\frac{G-1}{G}\right)\left(\frac{G+1}{3G}\right)\right), \\ &2)\ \text{Calculate } P_{MD} = F_{NC\chi^2}\left(\frac{\beta}{K_s+4K_b}; G, (K_s+4K_b)\, N_{\text{sym}} \left(\frac{G-1}{G}\right)\left(\frac{G+1}{3G}\right)\right). \end{aligned} \tag{116}$$

Comparing (116) with (95), it is evident that the ratio of the respective non-centrality parameters of the single UDC, multiple phase system to those of the multiple UDC, single phase system is $\left(\frac{G+1}{3G}\right)$. For all $G \in \mathbb{N}$, the factor $\left(\frac{G+1}{3G}\right)$ is less than unity and decreases monotonically with G. Asymptotically, we have $\left(\frac{G+1}{3G}\right) \to \frac{1}{3}$ as $G \to \infty$. As $\left(\frac{G+1}{3G}\right) < 1$ for all $G \geq 1$, it follows that the respective non-centrality parameters of the single UDC, multiple phase system are less than those of the multiple UDC, single phase one. Since it can be shown that the missed detection probability P_{MD} decreases as the respective non-centrality parameters increase [4], it follows that the multiple UDC, single phase system will always perform better than the corresponding single UDC, multiple phase one. Furthermore, as $\left(\frac{G+1}{3G}\right)$ is monotonic decreasing with G, it follows that the single UDC, multiple phase system will reach a point of diminishing returns more rapidly than the corresponding multiple UDC, single phase system [4]. This is evidenced upon comparing Fig. 14 with Fig. 15.

Despite the fact that a multiple UDC, single phase system outperforms a corresponding single UDC, multiple phase type scheme for a fixed detection time, there are advantages to using a single UDC, multiple phase system for signal detection. Specifically, if there is some leeway with respect to increasing the detection time, then there are several benefits to a single UDC, multiple phase type implementation. One such benefit is that while it is difficult to increase the number of UDCs in a multiple UDC, single phase system in a practical setting as it requires additional hardware, it is very simple to increase the number of timing phases of a single UDC, multiple phase system, as the only changes required are to trigger, store, and process the UDC test statistics at the different timing phases. At the expense of an increase in detection time, the improvement in performance is dramatic and is the result of both an increased detection time, as well as the number of timing phases.

For example, suppose that initially, $G = 2$ timing phases are used in a single UDC, multiple phase system and that for some given detection time that the missed detection probability is deemed excessively large. To improve the detection performance, we can, for instance, trigger the UDC to accumulate additional statistics at 3 times finer resolution to obtain an effective number of $G = 6$ timing phases. This only requires $6 - 2 = 4$ additional UDC test statistics at different timing phases. In essence, from an initial detection time of T_d using $G = 2$ phases, we arrive at a final detection time of $3T_d$ using $G = 6$ phases. Thus, the benefits of an increased detection time are twofold: an inherent improvement in performance as a result of the increased detection time as well as an additional improvement due to the increased number of timing phases.

From a practical point of view, perhaps the most efficient manner in which to increase the number of timing phases is to do so in powers of 2 until the missed detection probability performance is deemed acceptable. Specifically, starting from $G = 1$ timing phase, we double the timing resolution at each stage by accumulating additional UDC statistics as required until the missed detection performance is below its target requirement. At the k-th stage of such a detection scheme, the number of timing phases is $G = 2^{k-1}$, while the detection time is $T_d = 2^{k-1}T_{d,0}$, where $T_{d,0}$ denotes the nominal detection time per phase.

In summary, there are several pros and cons to using both of the proposed uplink signal detection schemes. While a multiple UDC, single phase system offers improved performance over a corresponding single UDC, multiple phase system for a fixed detection time, it requires additional hardware and cannot easily accommodate increased timing resolution. On the other hand, a single UDC, multiple phase system is amenable to increased timing resolution, provided that there is sufficient leeway with regards to increasing the detection time. Of course, with an implementation consisting of a fixed number of multiple UDCs, improved performance could also be obtained by using multiple timing phases instead of a single one. This would result in the most advantageous of all of the schemes considered, as it would result in the most detection information for a given detection time and number of UDCs.

VIII. Concluding Remarks

In this article, we focused on uplink signal detection for the DOT using the Neyman-Pearson hypothesis test. Specifically, we considered this hypothesis test for two different sets of test statistics: those from a multiple UDC, single phase system as well as those from a single UDC, multiple phase type implementation. Conditioned on a WCS symbol timing offset, we derived the performance of the Neyman-Pearson test for both sets of statistics, and assessed the advantages and disadvantages of both detection schemes.

For specific test cases (namely the dual UDC, single phase and single UDC, dual phase systems), we showed the problems inherent with deriving the performance of the *bona fide* unconditional Neyman-Pearson test. In particular, we showed that determining the decision regions based on the likelihood criterion was intractable for both cases. Future work involves assessing the performance of a suboptimal Neyman-Pearson type test using the conjectured decision regions given by (69) and (76) for the dual UDC, single phase and single UDC, dual phase schemes, respectively. In addition, it would be worthwhile carrying out similar analysis for the more general multiple UDC, single phase and single UDC, multiple phase systems.

References

[1] R. M. Gagliardi and S. Karp, *Optical Communications*, 2nd ed. New York, NY: John Wiley & Sons, Inc., 1995.

[2] H. P. Hsu, *Schaum's Outline of Theory and Problems of Probability, Random Variables, and Random Processes*, ser. Schaum's Outline. United States of America: McGraw-Hill Companies, Inc., 1997.

[3] P. P. Vaidyanathan, *Multirate Systems and Filter Banks*. Englewood Cliffs, NJ: Prentice Hall PTR, 1993.

[4] G. E. Corazza, Ed., *Digital Satellite Communications*. New York, NY: Springer Science+Business Media, LLC, 2007.

[5] M. K. Simon, S. M. Hinedi, and W. C. Lindsey, *Digital Communication Techniques: Signal Design and Detection*. Upper Saddle River, NJ: Prentice Hall PTR, 1995.

[6] K. J. Quirk, J. W. Gin, and M. Srinivasan, "Optical PPM synchronization for photon counting receivers," in *Proc. Military Communications Conference (MILCOM 2008)*, vol. 1, San Diego, California, USA, Nov. 17–19, 2008, pp. 1–7.

[7] I. S. Gradshteyn and I. M. Ryzhik, *Table of Integrals, Series, and Products*, 7th ed., A. Jeffrey and D. Zwillinger, Eds. Burlington, MA: Academic Press, 2007.

[8] B. C. Levy, *Principles of Signal Detection and Parameter Estimation*. New York, NY: Springer Science+Business Media, LLC, 2008.

Appendix: Multivariate Gaussian Distribution Integral Over a Hypersphere

In this section, we prove the following result:

$$\int_{\boldsymbol{x}\in\mathbb{R}^G:||\boldsymbol{x}-\boldsymbol{x}_C||^2<r^2} \frac{1}{(2\pi)^{\frac{G}{2}}} e^{-\frac{1}{2}||\boldsymbol{x}||^2}\, d\boldsymbol{x} = F_{NC\chi^2}\left(r^2; G, ||\boldsymbol{x}_C||^2\right) . \tag{A-1}$$

Note that the integrand in (A-1) is the pdf of a multivariate Gaussian or normal distribution with $\mathcal{N}_G(\mathbf{0}, \mathbf{I})$, which is a generalization of the *standard* normal distribution to the multivariate case [2]. Also, it should be noted that the region of integration in (A-1) is a *hypersphere* in $\mathbb{R}^G$ [8]. As seen in Sec. VI, this integral arises when deriving and assessing the performance of the Neyman-Pearson hypothesis test for uplink signal detection, conditioned on a particular value of the symbol timing offset.

In deriving (A-1), we will use the following result regarding the change of variables of a multidimensional integral [7]. Suppose that $\mathbf{u}$ and $\mathbf{v}$ are two $G \times 1$ vectors in $\mathbb{R}^G$ related by $\mathbf{v} = \varphi(\mathbf{u})$, where φ is an injective, differentiable function with continuous partial derivatives [7]. Furthermore, suppose U and V are two open sets in $\mathbb{R}^G$ such that $\varphi : U \to V$. Then, we have the following [7]:

$$\int_V f(\mathbf{v})\, d\mathbf{v} = \int_U f(\varphi(\mathbf{u}))\, |\det(\mathbf{J}(\varphi(\mathbf{u})))|\, d\mathbf{u}\,, \tag{A-2}$$

where $\mathbf{J}(\varphi(\mathbf{u}))$ is the $G \times G$ *Jacobian matrix* [7] of the transformation $\mathbf{v} = \varphi(\mathbf{u})$ whose (k, ℓ)-th element is given by

$$[\mathbf{J}(\varphi(\mathbf{u}))]_{k,\ell} = \frac{\partial\,[\mathbf{v}]_k}{\partial\,[\mathbf{u}]_\ell}\,, 0 \le k \le G-1\,,\ 0 \le \ell \le G-1\,.$$

To begin deriving (A-1), consider the transformation $\boldsymbol{y} \triangleq \mathbf{U}\,(\boldsymbol{x} - \boldsymbol{x}_C)$, where $\mathbf{U}$ is a unitary, *Householder* transformation matrix [3] given by

$$\mathbf{U} \triangleq \mathbf{I} - 2\mathbf{w}\mathbf{w}^T\,,\ \text{where}\ \mathbf{w} \triangleq \frac{\boldsymbol{x}_C + ||\boldsymbol{x}_C||\,\mathbf{e}_0}{||\boldsymbol{x}_C + ||\boldsymbol{x}_C||\,\mathbf{e}_0||}\,, \tag{A-3}$$

where $\mathbf{e}_0$ denotes the 0th unit vector [3] which is unity in the 0th component and zero otherwise. (More generally, $\mathbf{e}_k$ denotes the k-th unit vector [3] which is unity in the k-th component and zero otherwise.) As $\mathbf{U}$ is a real unitary matrix, we have $\mathbf{U}^T\mathbf{U} = \mathbf{U}\mathbf{U}^T = \mathbf{I}$ [3], and so $\boldsymbol{x} = \mathbf{U}^T\boldsymbol{y} + \boldsymbol{x}_C = \mathbf{U}^T\,(\boldsymbol{y} - \boldsymbol{y}_C)$, where $\boldsymbol{y}_C \triangleq -\mathbf{U}\boldsymbol{x}_C$. From this relation, it is clear that the Jacobian matrix is $\mathbf{J}(\varphi(\boldsymbol{y})) = \mathbf{U}^T$, and so $|\det(\mathbf{J}(\varphi(\boldsymbol{y})))| = 1$ as $\mathbf{U}$ is unitary [3]. Letting $\mathcal{I}$ denote the left hand side of (A-1) and appealing to (A-2), we get

$$\mathcal{I} \triangleq \int_{\boldsymbol{x}\in\mathbb{R}^G:||\boldsymbol{x}-\boldsymbol{x}_C||^2<r^2} \frac{1}{(2\pi)^{\frac{G}{2}}} e^{-\frac{1}{2}||\boldsymbol{x}||^2}\, d\boldsymbol{x} = \int_{\boldsymbol{y}\in\mathbb{R}^G:||\boldsymbol{y}||^2<r^2} \frac{1}{(2\pi)^{\frac{G}{2}}} e^{-\frac{1}{2}||\boldsymbol{y}-\boldsymbol{y}_C||^2}\, d\boldsymbol{y}\,. \tag{A-4}$$

To simplify (A-4), note that the vector $\boldsymbol{y}_C$ has all zeros in it except for the 0th component.

In order to show this, recall that $\boldsymbol{y}_C = -\mathbf{U}\boldsymbol{x}_C$ and so from (A-3) we have

$$\begin{aligned}
\boldsymbol{y}_C &= -\boldsymbol{x}_C + 2\left(\mathbf{w}^T\boldsymbol{x}_C\right)\mathbf{w} = -\boldsymbol{x}_C + \frac{2\left[||\boldsymbol{x}_C||^2 + ||\boldsymbol{x}_C||\,[\boldsymbol{x}_C]_0\right]}{||\boldsymbol{x}_C + ||\boldsymbol{x}_C||\,\mathbf{e}_0||}\mathbf{w}\,, \\
&= -\boldsymbol{x}_C + \frac{2\left[||\boldsymbol{x}_C||^2 + ||\boldsymbol{x}_C||\,[\boldsymbol{x}_C]_0\right]}{||\boldsymbol{x}_C + ||\boldsymbol{x}_C||\,\mathbf{e}_0||^2}\left[\boldsymbol{x}_C + ||\boldsymbol{x}_C||\,\mathbf{e}_0\right]\,, \\
&= -\boldsymbol{x}_C + \frac{2\left[||\boldsymbol{x}_C||^2 + ||\boldsymbol{x}_C||\,[\boldsymbol{x}_C]_0\right]}{2\left[||\boldsymbol{x}_C||^2 + ||\boldsymbol{x}_C||\,[\boldsymbol{x}_C]_0\right]}\left[\boldsymbol{x}_C + ||\boldsymbol{x}_C||\,\mathbf{e}_0\right] = -\boldsymbol{x}_C + \boldsymbol{x}_C + ||\boldsymbol{x}_C||\,\mathbf{e}_0\,.
\end{aligned}$$

Thus, we have $\boldsymbol{y}_C = ||\boldsymbol{x}_C||\,\mathbf{e}_0$, and so indeed the only nonzero component of $\boldsymbol{y}_C$ is its 0th component. Substituting this into (A-4) and defining $y_k \triangleq [\boldsymbol{y}]_k$ for all $0 \le k \le G-1$ for notational convenience leads to

$$\begin{aligned}
\mathcal{I} &= \int_{\boldsymbol{y}\in\mathbb{R}^G:||\boldsymbol{y}||^2<r^2} \frac{1}{(2\pi)^{\frac{G}{2}}} e^{-\frac{1}{2}||\boldsymbol{y}-||\boldsymbol{x}_C||\mathbf{e}_0||^2}\,d\boldsymbol{y}\,, \\
&= \int_{\boldsymbol{y}\in\mathbb{R}^G:||\boldsymbol{y}||^2<r^2} \frac{1}{(2\pi)^{\frac{G}{2}}} e^{-\frac{1}{2}\left(||\boldsymbol{y}||^2 - 2||\boldsymbol{x}_C||y_0 + ||\boldsymbol{x}_C||^2\right)}\,d\boldsymbol{y}\,. \qquad \text{(A-5)}
\end{aligned}$$

To evaluate (A-5), consider the following *hyperspherical coordinate system* [8] transformation:

$$\begin{aligned}
y_0 &= \rho\cos(\phi_0)\,, \\
y_1 &= \rho\sin(\phi_0)\cos(\phi_1)\,, \\
y_2 &= \rho\sin(\phi_0)\sin(\phi_1)\cos(\phi_2)\,, \\
&\vdots \\
y_{G-2} &= \rho\sin(\phi_0)\sin(\phi_1)\cdots\sin(\phi_{G-3})\cos(\phi_{G-2})\,, \\
y_{G-1} &= \rho\sin(\phi_0)\sin(\phi_1)\cdots\sin(\phi_{G-3})\sin(\phi_{G-2})\,.
\end{aligned}$$

Here, ρ denotes the radial coordinate, while $\phi_0, \phi_1, \ldots, \phi_{G-2}$ represent the angular coordinates. In a more compact form, we have

$$y_k = \begin{cases} \rho\left[\prod_{\ell=0}^{k-1}\sin(\phi_\ell)\right]\cos(\phi_k)\,, & 0 \le k \le G-2 \\ \rho\left[\prod_{\ell=0}^{k-1}\sin(\phi_\ell)\right]\,, & k = G-1 \end{cases}\,, \qquad \text{(A-6)}$$

where all empty products are assumed to be equal to unity here. With the transformation given in (A-6), it can be shown that the differential $d\boldsymbol{y}$ satisfies [8]

$$d\boldsymbol{y} = \rho^{G-1}\sin^{G-2}(\phi_0)\sin^{G-3}(\phi_1)\cdots\sin^2(\phi_{G-4})\sin(\phi_{G-3})\;d\rho\,d\phi_0\,d\phi_1\,\cdots\,d\phi_{G-2}\,,$$

which can be expressed more compactly as

$$d\boldsymbol{y} = \rho^{G-1}\left[\prod_{\ell=0}^{G-2}\sin^{G-2-\ell}(\phi_\ell)\right]\,d\rho\,\left(\prod_{\ell=0}^{G-2}d\phi_\ell\right)\,. \qquad \text{(A-7)}$$

Using (A-6) and (A-7) in (A-5) and noting that $||\boldsymbol{y}||^2 < r^2$ corresponds to the region $0 \leq \rho < r, 0 \leq \phi_0 < \pi, 0 \leq \phi_1 < \pi, \ldots, 0 \leq \phi_{G-3} < \pi, 0 \leq \phi_{G-2} < 2\pi$ leads to

$$\begin{aligned}\mathcal{I} &= \int_{\rho=0}^{r}\int_{\phi_0=0}^{\pi}\int_{\phi_1=0}^{\pi}\cdots\int_{\phi_{G-3}=0}^{\pi}\int_{\phi_{G-2}=0}^{2\pi}\frac{1}{(2\pi)^{\frac{G}{2}}}e^{-\frac{1}{2}\left(\rho^2-2||\boldsymbol{x}_C||\rho\cos(\phi_0)+||\boldsymbol{x}_C||^2\right)} \\ &\quad\times\rho^{G-1}\left[\prod_{\ell=0}^{G-2}\sin^{G-2-\ell}(\phi_\ell)\right]d\rho\left(\prod_{\ell=0}^{G-2}d\phi_\ell\right).\end{aligned}$$

This can be simplified to

$$\begin{aligned}\mathcal{I} &= \int_{\rho=0}^{r}\frac{\rho^{G-1}}{(2\pi)^{\frac{G}{2}}}e^{-\frac{1}{2}\left(\rho^2+||\boldsymbol{x}_C||^2\right)}\int_{\phi_0=0}^{\pi}e^{||\boldsymbol{x}_C||\rho\cos(\phi_0)}\sin^{G-2}(\phi_0) \\ &\quad\times\left[\prod_{\ell=1}^{G-3}\int_0^{\pi}\sin^{G-2-\ell}(\phi_\ell)\,d\phi_\ell\right]\left(\int_0^{2\pi}1\,d\phi_{G-2}\right)d\phi_0\,d\rho\,,\end{aligned}$$

which in turn can be simplified to the following:

$$\mathcal{I} = 2\pi\left(\prod_{\ell=1}^{G-3}\int_0^{\pi}\sin^{\ell}x\,dx\right)\left[\int_0^{r}\frac{\rho^{G-1}}{(2\pi)^{\frac{G}{2}}}e^{-\frac{1}{2}\left(\rho^2+||\boldsymbol{x}_C||^2\right)}\left(\int_0^{\pi}e^{||\boldsymbol{x}_C||\rho\cos\phi}\sin^{G-2}\phi\,d\phi\right)d\rho\right]. \tag{A-8}$$

In order to continue further with the simplification of $\mathcal{I}$, we will first use the following result from [7, pg. 397]:

$$\int_0^{\pi}\sin^{\nu-1}x\cos(ax)\,dx = \frac{\pi\cos\left(\frac{a\pi}{2}\right)}{2^{\nu-1}\nu B\left(\frac{\nu+a+1}{2},\frac{\nu-a+1}{2}\right)},\ \mathrm{Re}\left[\nu\right] > 0\,,$$

where $B(x,y)$ is the *beta function* [7]. Setting $\nu = \ell+1$ and $a = 0$ yields

$$\int_0^{\pi}\sin^{\ell}x\,dx = \frac{\pi}{2^{\ell}\left(\ell+1\right)B\left(\frac{\ell}{2}+1,\frac{\ell}{2}+1\right)}. \tag{A-9}$$

But from [7, pg. 909], we have $B(x,y) = \frac{\Gamma(x)\Gamma(y)}{\Gamma(x+y)}$, where $\Gamma(x)$ is the *gamma function* [7], and so $B(x,x) = \frac{(\Gamma(x))^2}{\Gamma(2x)}$. By the *doubling formula* for the gamma function [7, pg. 896], we have $\Gamma(2x) = \frac{2^{2x-1}}{\sqrt{\pi}}\Gamma(x)\,\Gamma\left(x+\frac{1}{2}\right)$, and thus $B(x,x) = \frac{\sqrt{\pi}\,\Gamma(x)}{2^{2x-1}\Gamma\left(x+\frac{1}{2}\right)}$. Substituting this into (A-9) leads to

$$\int_0^{\pi}\sin^{\ell}x\,dx = \frac{\sqrt{\pi}\,\Gamma\left(\frac{\ell+1}{2}+1\right)}{\left(\frac{\ell+1}{2}\right)\Gamma\left(\frac{\ell}{2}+1\right)}.$$

Now, as $\Gamma(x+1) = x\,\Gamma(x)$ [7, pg. 895], we have

$$\int_0^{\pi}\sin^{\ell}x\,dx = \sqrt{\pi}\,\frac{\Gamma\left(\frac{\ell-1}{2}+1\right)}{\Gamma\left(\frac{\ell}{2}+1\right)}, \tag{A-10}$$

and hence

$$\prod_{\ell=1}^{G-3}\int_0^{\pi}\sin^{\ell}x\,dx = \pi^{\left(\frac{G}{2}-\frac{3}{2}\right)}\cdot\frac{\Gamma(1)}{\Gamma\left(\frac{G}{2}-\frac{1}{2}\right)} = \frac{\pi^{\left(\frac{G}{2}-\frac{3}{2}\right)}}{\Gamma\left(\frac{G}{2}-\frac{1}{2}\right)}. \tag{A-11}$$

Here, (A-11) follows from the fact that the gamma function terms in (A-10) form a *telescoping product* [7] and the fact that $\Gamma(1) = 1$ [7, pg. 897].

Returning to (A-8), it follows that substituting (A-11) yields the following:

$$\mathcal{I} = \frac{2\pi^{\left(\frac{G}{2}-\frac{1}{2}\right)}}{\Gamma\left(\frac{G}{2}-\frac{1}{2}\right)} \int_0^r \frac{\rho^{G-1}}{(2\pi)^{\frac{G}{2}}} e^{-\frac{1}{2}\left(\rho^2+||\boldsymbol{x}_C||^2\right)} \left(\int_0^\pi e^{||\boldsymbol{x}_C||\rho\cos\phi} \sin^{G-2}\phi \, d\phi \right) d\rho \,. \tag{A-12}$$

To simplify the inner integral, note that from [7, pg. 491] that we have

$$\int_0^\pi e^{\pm\beta\cos x} \sin^{2\nu} x \, dx = \sqrt{\pi} \left(\frac{2}{\beta}\right)^\nu \Gamma\left(\nu+\frac{1}{2}\right) I_\nu(\beta) \;,\; \mathrm{Re}\left[\nu\right] > -\frac{1}{2} \,,$$

where $I_\nu(x)$ is the *modified Bessel function of the first kind* of order ν [7]. Setting $\beta = ||\boldsymbol{x}_C||\,\rho$ and $\nu = \frac{G}{2}-1$ yields

$$\int_0^\pi e^{||\boldsymbol{x}_C||\rho\cos\phi} \sin^{G-2}\phi \, d\phi = \sqrt{\pi} \left(\frac{2}{||\boldsymbol{x}_C||\,\rho}\right)^{\frac{G}{2}-1} \Gamma\left(\frac{G}{2}-\frac{1}{2}\right) I_{\frac{G}{2}-1}(||\boldsymbol{x}_C||\,\rho) \;.$$

Substituting this result into (A-12) leads to

$$\mathcal{I} = ||\boldsymbol{x}_C||^{-\frac{G}{2}+1} \int_0^r \rho^{\frac{G}{2}} e^{-\frac{1}{2}\left(\rho^2+||\boldsymbol{x}_C||^2\right)} I_{\frac{G}{2}-1}(||\boldsymbol{x}_C||\,\rho) \; d\rho \,. \tag{A-13}$$

Let $u \triangleq \rho^2$, so that $\rho = \sqrt{u}$ and thus $d\rho = \frac{1}{2}u^{-\frac{1}{2}}\,du$. Then, with this change of variables applied to (A-13), we get

$$\mathcal{I} = \int_0^{r^2} \underbrace{\left[\frac{1}{2} e^{-\frac{1}{2}\left(u+||\boldsymbol{x}_C||^2\right)} \left(\frac{u}{||\boldsymbol{x}_C||^2}\right)^{\frac{G}{4}-\frac{1}{2}} I_{\frac{G}{2}-1}\left(\sqrt{||\boldsymbol{x}_C||^2\, u}\right) \right]}_{f_{NC\chi^2}\left(u;G,||\boldsymbol{x}_C||^2\right)} du \,,$$

where $f_{NC\chi^2}\left(u; G, ||\boldsymbol{x}_C||^2\right)$ is the pdf of a noncentral chi-square distribution evaluated at u with G degrees of freedom and non-centrality parameter $||\boldsymbol{x}_C||^2$ [4]. As the cdf of any distribution is simply the integral of the associated pdf from $-\infty$ to the point of interest [2], and since the region of support of a noncentral chi-square random variable is $[0,\infty)$ [4], we have

$$\mathcal{I} = F_{NC\chi^2}\left(r^2; G, ||\boldsymbol{x}_C||^2\right) \;, \tag{A-14}$$

and so (A-14) and (A-4) imply (A-1). This completes the proof.